UNIVERSITY OF CALIFORNIA SAN DIEGO

Neuroinflammation in Alzheimer's Disease Contributes to A2-type Reactive Astrocytic Profile in iPSC Derived Patient Astrocytes

A Thesis submitted in partial satisfaction of the requirements for the degree Master of Science

in

Biology

by

Lauren T. Hui

Committee in charge:

Professor Fred H. Gage, Chair
Professor Yishi Jin, Co-Chair
Professor Ashley Juavinett

2021

The thesis of Lauren T. Hui is approved, and it is acceptable in quality and form for publication on microfilm and electronically.

University of California San Diego

2021

DEDICATION

For my family, who have always supported and encouraged me to pursue my dreams.

TABLE OF CONTENTS

LIST OF ABBREVIATIONS

Alzheimer's Disease - AD

Early-Onset Alzheimer's Disease - EOAD

Late-Onset Alzheimer's Disease - LOAD

Ribonucleic Acid - RNA

Induced Pluripotent Stem Cells - iPSCs

Central Nervous System - CNS

Amyloid Precursor Protein - APP

Amyloid-Beta Peptide - Aβ

Sendai Virus - SeV

Principal Component Analysis - PCA

Differentially Expressed Genes - DEGs

Log2 Fold Change – LogFC or LFC

LIST OF FIGURES

LIST OF SUPPLEMENTAL FIGURES AND TABLES

ACKNOWLEDGEMENTS

Thank you to the following individuals without whom this thesis would not have been possible:

Dr. Fred Gage and the Gage lab, who gave me the opportunity to research, be trained, and conduct my MS in his lab

Dr. Yishi Jin, who encouraged my research and pursuit of higher education and teaching

Dr. Ashley Juavinett, who gave me the training and courage to explore data science and bioinformatics

Dr. Jeffrey Jones, my wonderful postdoctoral mentor and teacher

Dr. Ioana Nitulescu and Desiree Ramirez

Dr. Nichola Allen and Allen lab

Fan Qiu, who patiently taught me how to align my reads remotely

Lynne Moore, who welcomed me to the Gage lab

Beth Coyne, who patiently responded to all my panicked inquiries throughout my MS degree

ABSTRACT OF THE THESIS

Neuroinflammation in Alzheimer's Disease Contributes to A2-type Reactive Astrocytic Profile in iPSC Derived Patient Astrocytes

by

Lauren T. Hui

Master of Science in Biology

University of California San Diego, 2021

Professor Fred H. Gage, Chair
Professor Yishi Jin, Co-Chair

Alzheimer's disease (AD) is a progressive neurodegenerative disease characterized by loss of neurons and synapses throughout the brain. Increased neuroinflammation has been observed in the brains of AD patients and is hypothesized to play a role in the pathology of the disease. Inflammation in the brain is thought to be primarily initiated by the non-neuronal cells of the brain, glia cells. One type of glia, astrocytes, are suspected to play a role in the onset and progression of AD through inflammation. Recent characterization of reactive astrocytes has identified two activated astrocyte states: a harmful, pro-inflammatory A1 state or a helpful, anti-inflammatory A2 state when exposed to CNS injury. In this thesis, I asked if A1 or A2 astrocyte states were different between AD and control astrocytes. Here, I analyzed RNA-sequencing data

from AD astrocytes generated from patient-derived induced pluripotent stem cells (iPSCs) along with age-matched controls to identify the relative proportions of A1 and A2 states. Surprisingly, I found that AD astrocytes have an increase in A2-type, “helpful” astrocytes relative to age-matched cognitively normal controls. These results reflect the complexity of AD and suggest new ways of thinking about inflammation in AD.

INTRODUCTION

The aim of this thesis is to characterize the inflammation status of astrocytes in Alzheimer's disease (AD), utilizing RNA-sequencing data from astrocytes derived from patient induced pluripotent stem cells (iPSCs). Our dataset is composed of 3 differentiations of astrocytes each from 6 individuals: 3 with AD and 3 cognitively normal, aged-matched controls.

Reactive astrocytes likely play a significant role modulating neuroinflammation in AD, by influencing disease progression and severity of symptoms related to the disease (Glass et al. 2010). Furthermore, known familial mutations associated with AD, such as *PSEN1*, have been shown to alter astrocyte behavior and core astrocytic functions and compromises their ability to support neurons in AD (Oksanen et al. 2017). Central nervous system (CNS) injury studies have proposed different activation states for astrocytes that can range from harmful (A1) to helpful (A2), which upregulate pro-inflammatory or anti-inflammatory responses (Liddleow et al. 2017). I hypothesized that the harmful reactive state of astrocytes (A1) is implicated in exacerbating the inflammatory response in AD and would exhibit differential gene expression in their transcriptome compared to controls.

BACKGROUND

1. Alzheimer's Disease

Alzheimer's disease (AD) is a complex age-related neurodegenerative disorder with both sporadic and familial forms; it is characterized by a progressive decline in cognitive abilities such as memory, language, personality, and behavior, leading to dementia and eventually death (Weller and Budson 2018). It is estimated that over 50 million people worldwide have dementia, and of those, 60-70% of cases can be attributed to AD. AD not only affects patients, but their families and caregivers, who face rising costs of care as well as emotional and physical

difficulties associated with being a long-term caregiver. Up to 10 million new cases are reported each year, making it one of the most pressing health concerns today for the world's aging population (Alzheimer's Association 2020).

Multiple clinical diagnostic criteria have been established to diagnose AD at different stages: early preclinical with no symptoms, a middle stage with mild cognitive impairment, and a final stage with symptoms of dementia ("Alzheimer's Disease Diagnostic Guidelines" n.d.). These stages and their severity are assessed with cognitive assessments in combination with biomarker tests, where prior to 1984, the only confirmation of diagnosis was post-mortem ("Alzheimer's Disease Diagnostic Guidelines" n.d.) Cognitive impairment can be assessed by administering a combination of tests including the Montreal Cognitive Assessment (MoCA), Mini-Mental State Examination (MMSE), and Braak staging, a method to quantify the prevalence of proteinaceous aggregates per area in the patient brain on a scale of (I-IV) (Adler et al. 2019). A combination of magnetic resonance imaging (MRI), hypometabolism on fluorodeoxyglucose (FDG) positron emission tomography (PET), and hypoperfusion on single-photon emission tomography (SPECT) have shown abnormalities in the brain prior to cognitive impairment (Cummings 2012).

95% of AD cases are sporadic, meaning they have no known familial genetic cause, and only about 5% of AD cases are attributable to a familial cause from a heritable genetic mutation (Bali et al. 2012). Historically, sporadic AD has been understudied since animal models do not sporadically develop AD; most studies utilize models with known familial AD mutations. This study utilizes cells generated from sporadic-onset patients diagnosed with AD, which gives unique and new insight into the transcriptomes of astrocytes from sporadic AD patients.

However, it is unknown whether the patients had any familial AD-related mutations, or the patients' overall protein load or ApoE status at time of cell collection.

Historically AD has been diagnosed post-mortem by the presence of extracellular amyloid beta plaques and intracellular tau neurofibrillary tangles, pathological hallmarks. The exact pathogenesis of AD is not known. Pathological hallmarks suggest that Aβ and hyper-phosphorylated tau are involved in late-stage AD, although a causal link is still debatable. Mutations in several genes of interest increase the risk of developing AD, including inheritable familial mutations. Familial AD is typically caused by mutations in the gene for amyloid precursor protein (APP) or mutations in presenilin genes *PSEN1* and *PSEN2*, whose protein products participate in processing APP (Dorszewska et al. 2016). Mutations in APP processing leads to buildup of amyloid plaques and impairs clearance of the proteins, leading to the pathological amyloid beta plaques associated with AD. Several genetic factor risk factors for developing AD have been found, such as the ε4 allele of ApoE, which also increases risk of earlier age of onset (van der Lee et al. 2018).

The APP gene has 18 exons which may be alternatively spliced, producing 10 different isoform products from 563 to 770 amino acids in length. The APP 695 product is predominant in the central nervous system of healthy patients and is cleaved by the gamma secretase complex to produce the amyloid-beta peptide (Aβ), typically 39 to 42 amino acids long (Kelleher and Shen 2017). The gamma secretase complex is a common site of mutation, and the effects of mutation are seen in familial AD (Piaceri, Nacmias, and Sorbi 2013). The gamma secretase complex is made up of four proteins: nicastrin, presenilin-1, PEN-2, and APH-1. Of these, presenilin-1 is one of the most common sites of mutation, with the PSEN1/PSEN2 gene mutations being some of the most well-known genetic causes of AD due to it causing increased production of Aβ42 or

enhanced APP processing (Kelleher and Shen 2017). The size of Aβ is utilized as a marker of abnormal APP processing: Aβ40 is the common isoform seen in healthy patients whereas Aβ42, the longer variant, is highly susceptible to amyloid fibrillogenesis and is upregulated in familial AD.

2. Inflammation in AD

A common theme of AD is the presence of neuroinflammation, regardless of whether it manifests as familial or sporadic AD. The exact mechanism by which inflammation is mediated in AD is unclear, but it has been tied primarily to Aβ peptides, neurofibrillary tangles, and overall neuronal degeneration, all of which are hallmarks of AD shown in models and in postmortem tissue (Neuroinflammation Working Group et al. 2000). Inflammation appears to have both neuroprotective and detrimental qualities: in acute responses, it appears to be neuroprotective, but when it becomes chronic, inflammation can become detrimental (Kim and Joh 2006; Kinney et al. 2018).

It is hypothesized that Aβ peptides activate microglia, which are responsible for releasing pro-inflammatory products, including reactive oxygen species (ROS), nitric oxide, and cytokines, which can then activate astrocytes and cause astrogliosis and further inflammatory responses (Baik et al. 2016). Specific cytokines have been associated with inflammatory signaling in AD, including TNF-α, IL-1β, IL-6, NFκB, IL-10, and TGF-β (Kinney et al. 2018). This sustained immune response and inflammation can further damage neurons, which continues a feed-forward response that activates microglia and causes additional cytokine release, inflammation, and contributes to neurodegeneration (Hickman, Allison, and El Khoury 2008)

New studies have revealed that the innate immune system contributes to formation of amyloid plaques via γ-secretase modulation (Hur et al. 2020). As previously discussed, γ-

secretase activity is critical to AD development as it regulates production of Aβ peptides. Interferon-induced transmembrane proteins were recently identified as novel regulators of γ-secretase, pointing to a greater role of the immune system and cytokine release in AD progression (Hur et al. 2020). This led me to hypothesize that immune system-related genes and inflammation-related genes would be significantly upregulated in AD vs control astrocytes.

3. iPSC generation and current methods of AD modelling

Induced human pluripotent stem cells (iPSC) have proved effective in modelling disease pathology since their discovery in 2007. iPSCs provide a human-specific primary cell culture system to complement existing animal models. Because iPSCs are derived directly from patient cells, translating findings to the clinic are now more possible than ever, and was chosen for this study as it allows us to examine sporadic-onset AD, which has been historically understudied due to a lack of appropriate models. The iPSC system allows researchers to generate nearly every cell type in the human body and observe disease states *in vitro*. Since iPSCs are infinitely expandable, they provide a major improvement to human tissue availability by providing a limitless source of samples that can be derived from a wide variety of patient cell-types, including blood and skin fibroblasts (Medvedev, Shevchenko, and Zakian 2010).

Reprogramming somatic cells, such as dermal fibroblasts, to a pluripotent state is achieved through only four transcriptional factors, Oct3/4, Sox2, c-Myc, and Klf4 (also known as the Yamanaka factors) (Yamanaka 2007). From iPSC stage, addition of reprogramming factors at specific timepoints has allowed researchers to induce a variety of cell types relevant to the diseases being studied.

The Yamanaka method is limited by several factors, including integration of exogenous viral transgenes into the host genome and low induction efficiency. Inserting retroviruses in the

genome increases the risk of tumorigenicity, and other methods of increasing induction efficiency were not able to resolve these issues (Medvedev, Shevchenko, and Zakian 2010). An alternate iPSC induction method was found in 2009 to resolve both these issues: the Sendai virus. The Sendai virus (SeV) is an RNA virus that carries no risk of altering the host genome; SeV vectors replicate in the cytoplasm as negative-sense single-stranded RNA, which does not interact with nor integrate into the host genome and has high efficiency relative to the Yamanaka method alone (Fusaki et al. 2009). Utilizing the SeV delivery system in conjunction with the Yamanaka factors allows for effective iPSC generation without risk of integration to the host genome, which is important for preserving the genetic hallmarks of disease pathology. The SeV delivery system is vital for generation of reliable *in vitro* cell models for research as it preserves endogenous genetic material while consistently supporting transformation vectors. In AD models, iPSCs generated from patient cells must remain unaltered by exogenous genes in order to preserve the endogenous factors contributing to the AD phenotype, including heritable risk factors.

The iPSC system has been used in studies of AD to model the progression of the disease, examine genetic risk factors, and provide a model for drug development and testing. In our experiment, the SeV delivery system was utilized to generate reactive astrocytes from confirmed AD patients and age-matched controls.

Astrocytes derived from iPSCs vary in terms of their functionality and morphology, largely dependent on the protocol used to generate them. It is generally accepted that astrocyte identifiers are stellate morphology and positive expression of S100β and glial fibrillary acidic protein (GFAP), though other markers such as A2B5 and CD44 may be used (Krencik and Zhang 2011). Functionality of astrocytes may be assessed by glutamate uptake, calcium

transients, and response to pro-inflammatory stimuli (Santos et al. 2017). Though there are no singularly definitive markers agreed upon for astrocytes, multiple markers and functionality assessments can and should be utilized to assess the quality and robustness of the differentiated astrocytes.

4. Astrocytes in AD, Astrocyte Reactivity

Astrocytes normally play a support role in the brain; they secrete small molecules to promote and maintain synapses, secrete protective antioxidants such as glutathione, supply nutrients to nervous tissue, regulate the blood-brain barrier, and play a role in repair and recovery after traumatic brain injury (Siracusa, Fusco, and Cuzzocrea 2019). Astrocytes also form scars after CNS injury and play a role in axon guidance and regeneration, which may be of interest for AD treatment since synapses are damaged in AD (Anderson et al. 2016). They are the most abundant type of glial cell and previous studies have reported that they comprise 20-40% of all glial cells (Verkhratsky and Butt 2013). When assessing astrocytes for function, calcium homeostasis, cytokine and antioxidant small molecule release, and glycolytic stress are often utilized as a benchmark.

Studies have been shown that astrocytes with the same genetic profile as AD patients have altered metabolism, altered cytokine release in pro-inflammatory conditions, and show an inability to propagate calcium transients (Oksanen et al. 2017). The immune system and complement cascade have been associated with abnormal clearing or development of Aβ and are considered a risk factor for AD (González-Reyes et al. 2017). This led us to theorize that altered astrocyte activity may be linked to pro-inflammatory activity or an altered response to inflammatory signalling, contributing to the progression of AD symptoms. Upregulation of pro-

inflammatory genes such as IL-6, IL-1β, NO, and TNFα have been previously associated with Aβ species, such as $A\beta_{1\text{-}42}$, implicated in AD (Lindberg et al. 2005; Hou et al. 2011).

It has been observed that two different astrocytic states arise post-spinal cord injury, termed A1 and A2 (Liddelow et al. 2017). Reactive microglia have been shown to induce an A1 state through release of cytokines IL-1α, TNF, and C1q, which causes the A1 state to lose essential astrocytic functions such as induction of excitatory synapses and phagocytic capacity (Liddelow et al. 2017). They are also highly neurotoxic to CNS neurons and mature oligodendrocytes, even when caspase-2 and caspase-3 inhibitors are added to cell culture. The transcriptome of A1 astrocytes demonstrate upregulation of H2-D1, IIGP1, PSMB8, SRGN, AMIGO2, SERPING1, GGTA1, HW-T23, GPP2, FKBP5, C3, and FBLN5 (Li et al. 2019). They have also been identified as present in other neurodegenerative diseases, such as Huntington's disease (Khakh et al. 2017), Parkinson's disease, amyotrophic lateral sclerosis, and multiple sclerosis (Liddelow et al. 2017). Aged astrocytes also take on a more A1-like reactive phenotype, which can be reduced in mice lacking microglial-secreted cytokines mentioned above. The aged astrocytes lose normal functions similar to A1-reactive astrocytes post-CNS injury, and may contribute to cognitive decline and vulnerability in critical brain regions (Clarke et al. 2018). Reportedly, complement component C3 is the most common and most characteristic upregulated gene expressed by A1 astrocytes, with up to 60% of GFAP+ astrocytes in the prefrontal cortex being C3+ in human AD tissue (Liddelow et al. 2017).

In contrast, the A2 state is neuroprotective and releases trophic factors that promote healing and repair of membranes and tissues. They have previously been associated with post-stroke ischemia and AQP4 to reabsorb excess fluid in brain edemas and to secrete small molecules to promote neurotrophic factors in the CNS (Zador et al. 2009; Papadopoulos et al.

2004). Upregulated A2 genes include Clcf1, Tgm1, Ptx3, S100a10, Sphk1, Cd109, Ptgs2, Emp1, Slc10a6, Tm4sf1, B3gnt5, Cd14, and Stat3 (Liddelow et al. 2017). Of these, S100a10 is particularly noteworthy for its role in promoting cell proliferation, membrane repair, and inhibition of apoptosis. S100a10 also promotes production of anti-inflammatory cytokine TGFβ, which participates in synaptogenesis and has a neuroprotective role (Li et al. 2019).

5. Summary of Thesis Aims

This thesis aims to explore the changes in the transcriptome of sporadic AD patient-derived astrocytes generated from iPSCs and compare them to those of age-matched controls. Sporadic AD has historically been understudied due to a lack of appropriate modelling systems and using the iPSC system provides new insight into sporadic forms of AD that may reveal differences or similarities to familial AD that have not been observed previously. Analysis of the differentially expressed genes may shed light on changes in cell function and signaling in AD astrocytes.

Additionally, this thesis aims to examine the transcriptome of astrocytes and their role in AD, as it has been shown that familial AD mutations can cause astrocyte dysfunction and disrupt neuronal homeostasis. The cause of neuroinflammation in AD is unknown, however, astrocytes are of interest as they play a role in the inflammation cascade. AD astrocytes may exhibit a more pro-inflammatory activated state than controls.

Lastly, this thesis examines whether astrocytes in AD more closely resemble the proposed A1 “harmful” or A2 “helpful” states as described previously in literature (Liddelow et al. 2017). Based on previous literature, I hypothesized that AD astrocytes more closely resemble the A1 “harmful” state which would show significant upregulation in the defined A1 genes compared to controls.

METHODS

Astrocyte Generation and RNA Extraction

Astrocytes were generated in triplicate from 3 stable patient-derived induced pluripotent stem cell lines and 3 age-matched controls as previously described (Santos et al. 2017). Briefly, iPSCs were differentiated into glia progenitor cells (GPCs) via embryoid body formation in the presence of 500ng/mL Noggin (Peprotech) for 2 weeks with 10ng/ml PDGFAA (R&D Systems) added for an additional week. Next, GPCs were dissociated to single cell and expanded as a monolayer in astrocyte medium (DMEM/F12 Glutamax with N2 and B27 [Thermo Fisher Scientific] with 10% fetal bovine serum [FBS, Omega Scientific]) with human 20ng/mL FGF2 for 2 weeks, and human 10ng/mL human LIF (Alomone Labs) supplemented for the last week.

RNA was extracted via Qiagen RNeasy kit and reverse-transcribed to cDNA via invitrogen SuperScript III. Samples were submitted to Illumina next-generation sequencing. SolexaQA++ was used to trim low quality reads and cutadapt to trim Illumina adapters.

RNA-seq Data Quality Control

Reads were mapped using StAR (Dobin et al. 2013) against the Genome Reference Consortium Human Build 38 (Schneider et al. 2016). Raw, unnormalized counts were obtained and analyzed using the DeSeq2 package (Love, Huber, and Anders 2014) and EdgeR packages (Y. Chen, Lun, and Smyth 2016). The apeglm package was utilized for LFC shrinkage (Zhu, Ibrahim, and Love 2019). A principal component analysis (PCA) was generated initially from raw, unnormalized counts using the DeSeq2 package and the pcaExplorer function to observe whether disease and control groups had a significant difference (Marini, Federico, and Binder 2019). Read counts and gene length bias were analyzed against a normal distribution using a dispersion plot generated with DeSeq2, then quality control was performed. Genes with raw

averaged expression less than 25 were removed, and remaining genes were filtered by p-value to remove any genes with p-value greater than 0.05. Log2fold change (LFC) was considered significant if greater than 1.5 and the identified genes were considered “differentially expressed genes (DEGs)”.

An MA plot was generated using DeSeq2 with all genes that passed quality control to visualize DEGs. Lastly, a Pearson correlation plot was generated with DeSeq2 to visualize and predict relationships between samples using both a heatmap and hierarchical clustering.

Differential Gene Expression Analysis

DEGs were then submitted to Enrichr and String-DB for gene ontology and protein-protein interaction analysis (E. Y. Chen et al. 2013; Kuleshov et al. 2016; Szklarczyk et al. 2019). Only upregulated DEGs were submitted to String-DB, and both upregulated and downregulated DEGs were submitted to Enrichr.

DEGs were also compared to existing pre-established gene families listed on Enrichr: “Inflammation” genes from Inflammation mediated by chemokine and cytokine signaling pathway Homo sapiens P00031 from Panther_2016 (188 genes); “Early Onset” genes from Alzheimer Disease, Early Onset from DisGeNET (115 genes); “Late Onset” genes from Alzheimer Disease, Late Onset from DisGeNET (252 genes); “Familial” genes from Familial Alzheimer Disease (FAD) from DisGeNET (187 genes). DEGs were also compared to A1 and A2 gene lists reported from literature (Liddelow et al. 2017).

RESULTS

Quality Control

The first priority of this project was to ensure quality of the data, and assess any variability between individual samples or between replicates. To accomplish this, a principal

component analysis was performed to reduce dimensionality across the cohorts to obtain an initial “snapshot” of the data sets without compromising the quality of data (Figure 1).

The principal component analysis (PCA), consisting of the 9 AD and 9 control samples, showed clear separation between the two axes, suggesting an observable difference between the AD and control data sets (Figure 1). The AD samples clustered along the left side of the X-axis , and the control groups clustered along the right side of the X-axis (PC1, 53% variance). Interestingly, there was also some separation between AD and control along the y-axis (PC2, 23% variance), although it was not as consistent. One control group clusters closer to the AD set than the other controls, suggesting an outlier that may be more AD-like than others. It has been previously observed that patients may be cognitively normal at time of sample collection but develop AD at a later point in time; this may have been the case of samples from this control patient, however, we cannot attribute this result conclusively as we lack the patient clinical data to confirm this finding (Supp. Figure 1). However, individual replicates from each group were consistently clustered together, supporting the robustness of the data set and consistency between

handling of replicates of each sample.

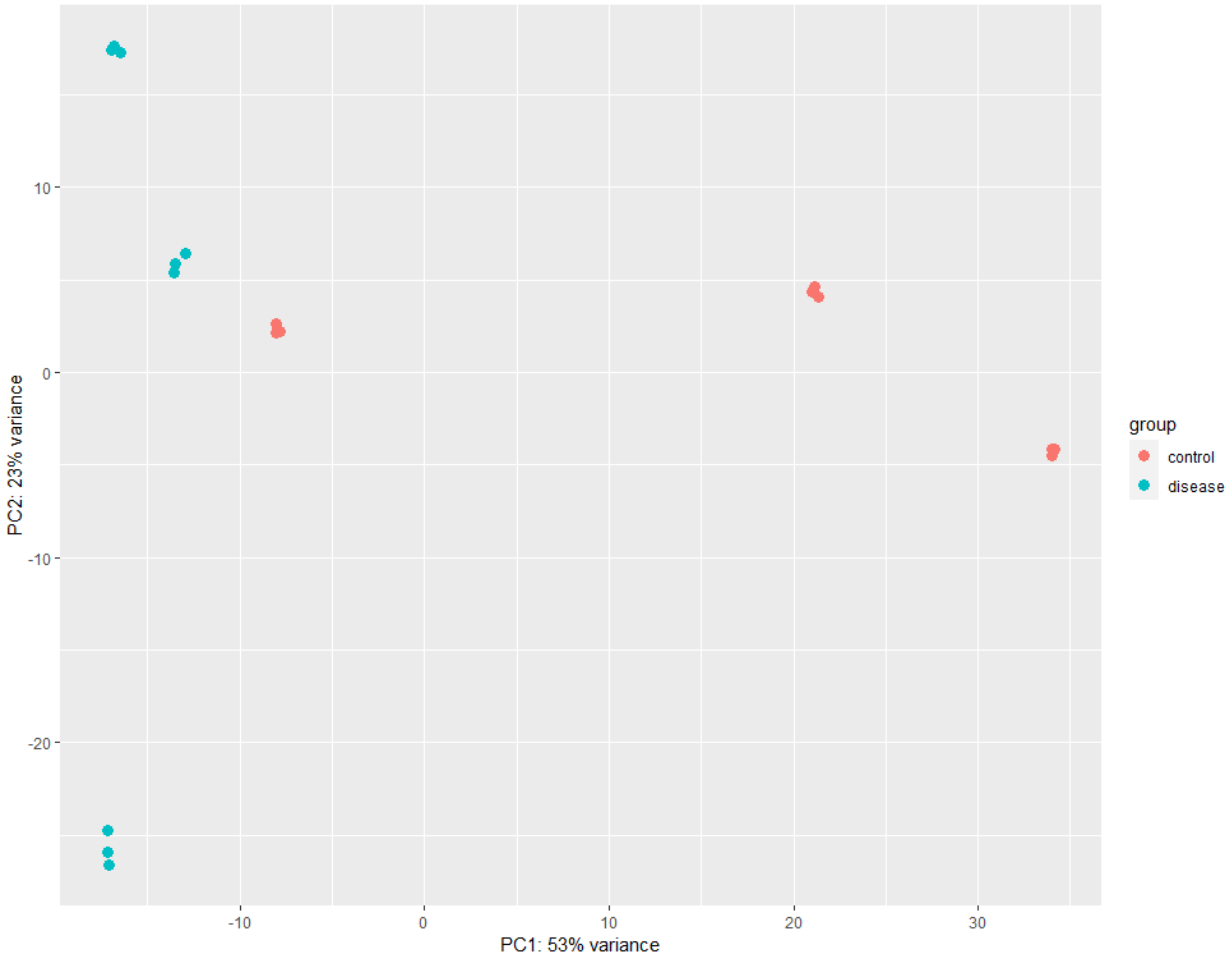

Figure 1: Principal component analysis of disease vs control samples reduced along two axes.

In order to investigate if differences in read depth accounted for any of the variability indicated by PCA, individual raw read counts were compared per sample. The raw, unnormalized read counts can be observed in Figure 2. The total counts for each group showed some minor variations between samples on a linear scale, but demonstrated good consistency between samples, suggesting that the quality and depth of the reads were consistent across all

samples.

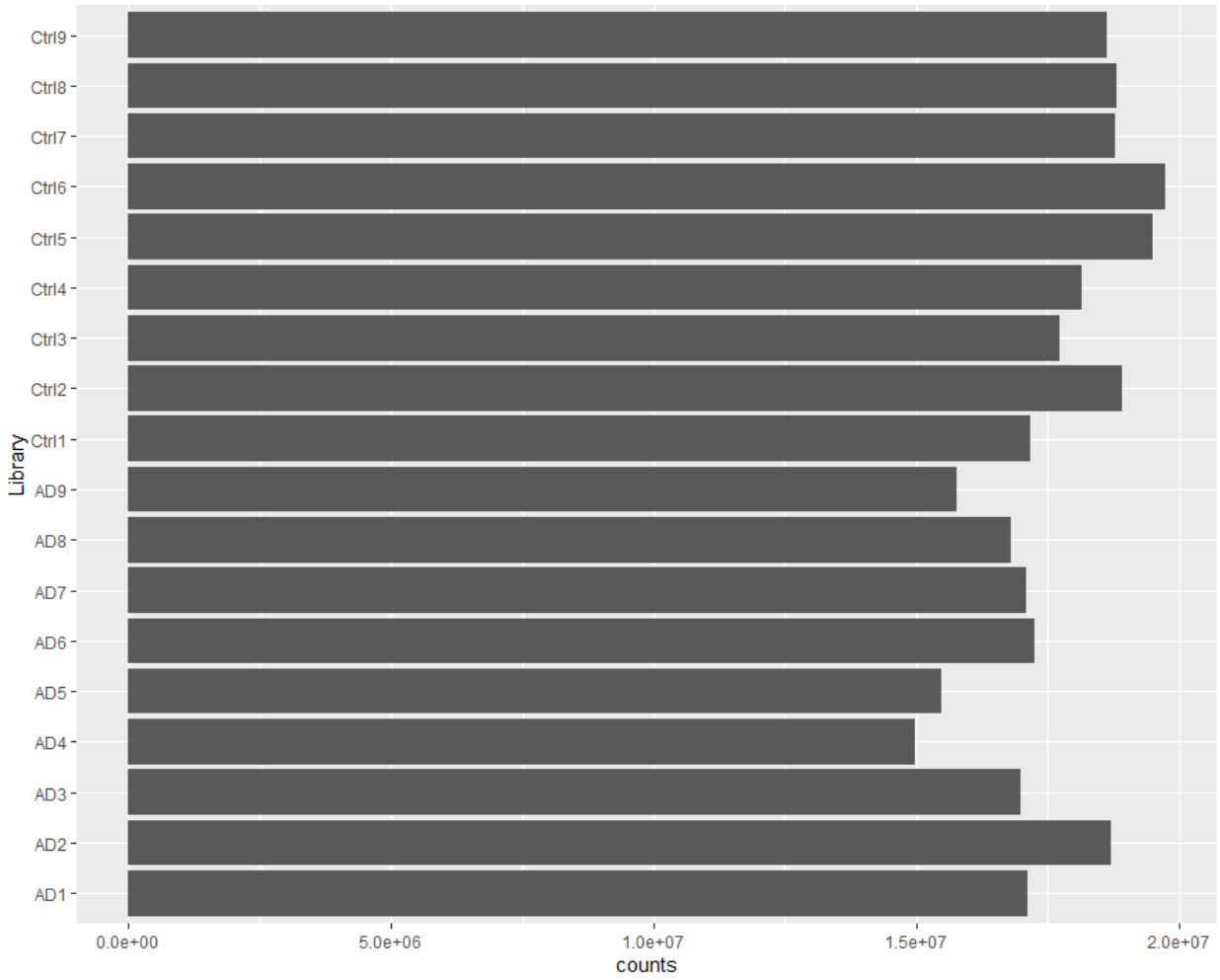

Figure 2: Individual read counts for all samples, approximately equal. AD samples have slightly fewer read counts that may be due to natural variations in number of cells submitted for signaling.

Normalizing the raw linear read-counts to log scale demonstrated that the reads were approximately equal for all samples that were sequenced (Figure 3). Counts from AD 7, 8, 9 replicates, had slightly fewer counts per million (log2 CPM), potentially suggesting variation in total RNA or cell number input, was not different enough to raise concern as this minor

difference did not affect this sample via PCA (Supp. Fig. 1).

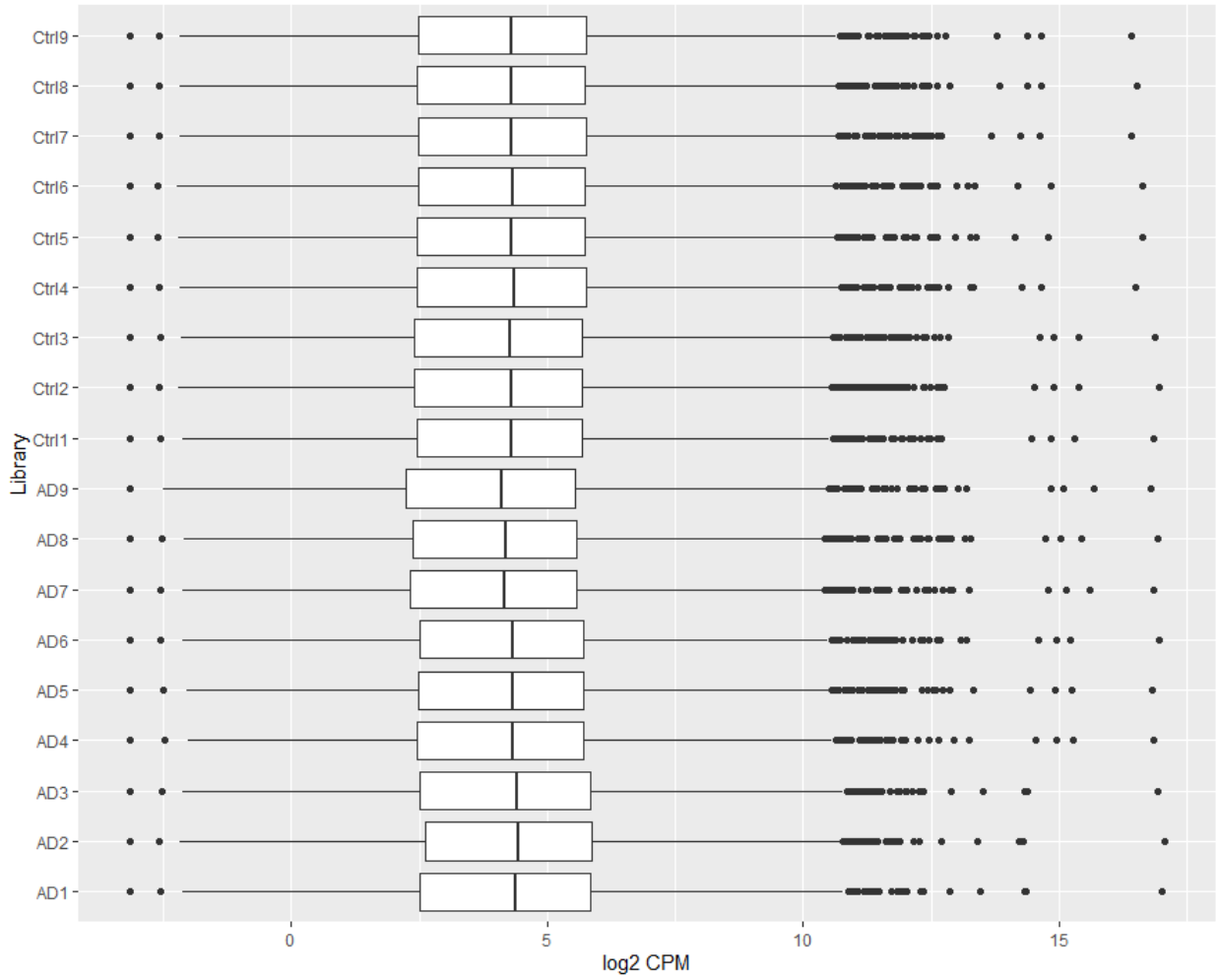

Figure 3: Normalized log2 counts per million for all samples.

Differential Expression Analysis

A dispersion plot was generated to control for read count (or gene length) bias to determine normalization of all genes relative to a best fit curve (Figure 4). The dispersion plot suggests there was a normal spread of gene counts along the axis of dispersion and that several genes (bold dots) do not fit the normalization model, suggesting a biological basis for dispersion. The analysis provides confidence in the underlying biology and removes potential artifacts of

sequencing, allowing for more analysis on our dataset.

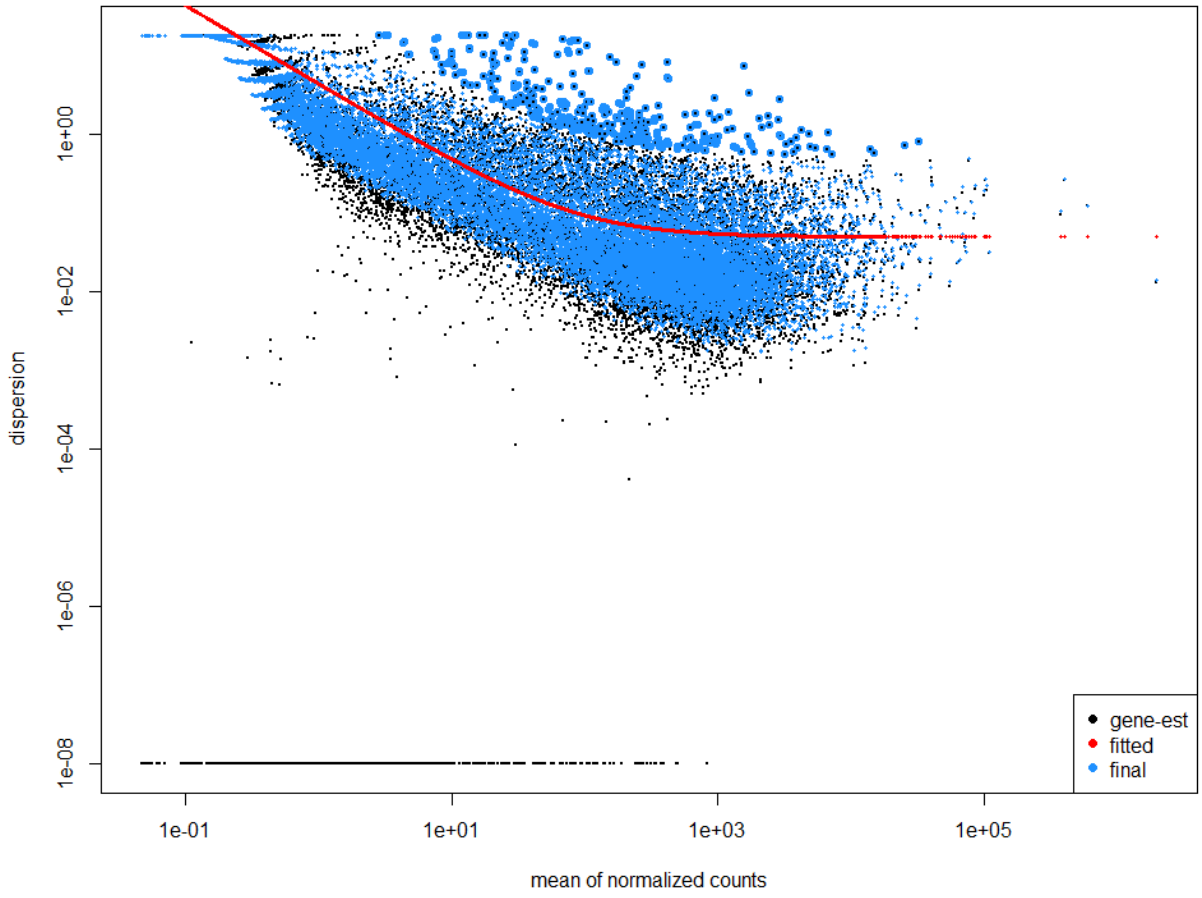

Figure 4: Dispersion plot generated to control for read count (or gene length) bias, showing the majority of counts fit along the normalization model.

Differential sequence analysis was performed after categorizing AD and control groups into “disease” versus “control”, respectively. Subsequent visualizations were generated using a variance-stabilizing transform of the data, which yielded the most stable normalization of the data (Supp. Fig. 1). Heatmap analysis of differential expression (Supp. Fig. 3) revealed consistent upregulation and downregulation of gene groups differentially between the disease and control groups.

Normalized gene counts were compared between AD and control groups using DeSeq2 to identify and analyze differential gene expression between the disease and control groups. These results were visualized via an MA-plot (Figure 5). The results suggest hundreds of statistically significant differentially expressed genes (DEGs; p-value ≤ 0.05) between AD and control groups across 13,454 genes that passed quality control. Of these genes, 1653 (12%) were significantly upregulated with a log fold change greater than 1.5, and 1933 (14%) were significantly downregulated with a log fold change less than 1.5.

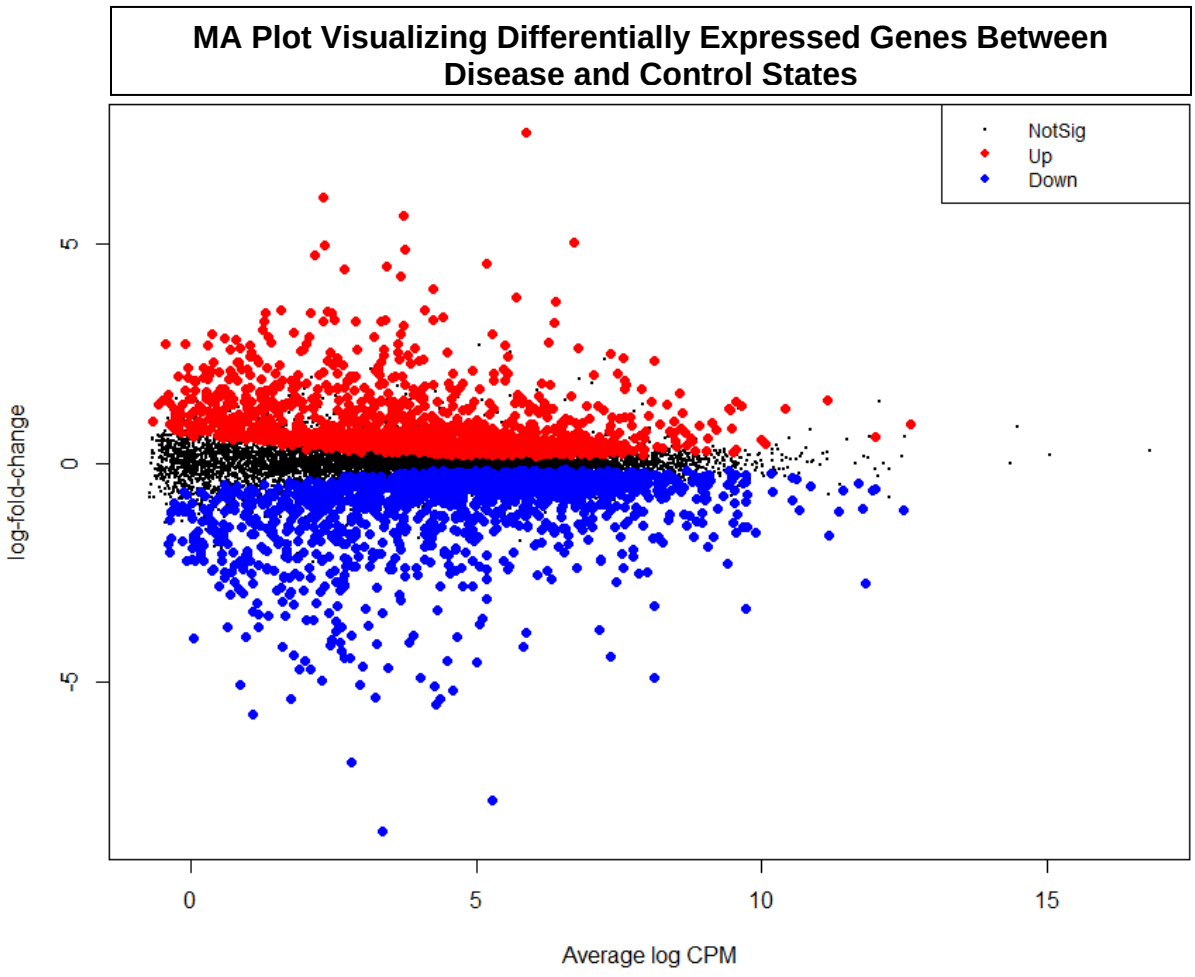

Figure 5: MA-plot visualizing differential expression analysis. Each dot represents a gene. Red dots are significantly upregulated, while blue dots are significantly downregulated. Black dots indicate non-significant log-fold change.

The relationships between the AD and control groups were examined via unbiased hierarchical clustering of DEGs. This analysis was visualized via Pearson's correlation heatmap (Figure 6). One cluster of controls were more similar to an AD "disease" group than the other control groups. This finding reflected our initial principal component analysis where AD replicates 4, 5, and 6 were closer to Ctrl 1, 2, and 3 replicates than other AD or Ctrl groups (Supp. Fig. 2). This may be due to the age-matched control sample being cognitively normal at time of sample collection but may have been diagnosed with AD or dementia after collection of the sample. However, this study lacks the clinical data needed to make such a conclusion; this suggests that RNA-seq data on iPSC derived AD astrocytes demonstrate an AD specific

transcriptomic profile.

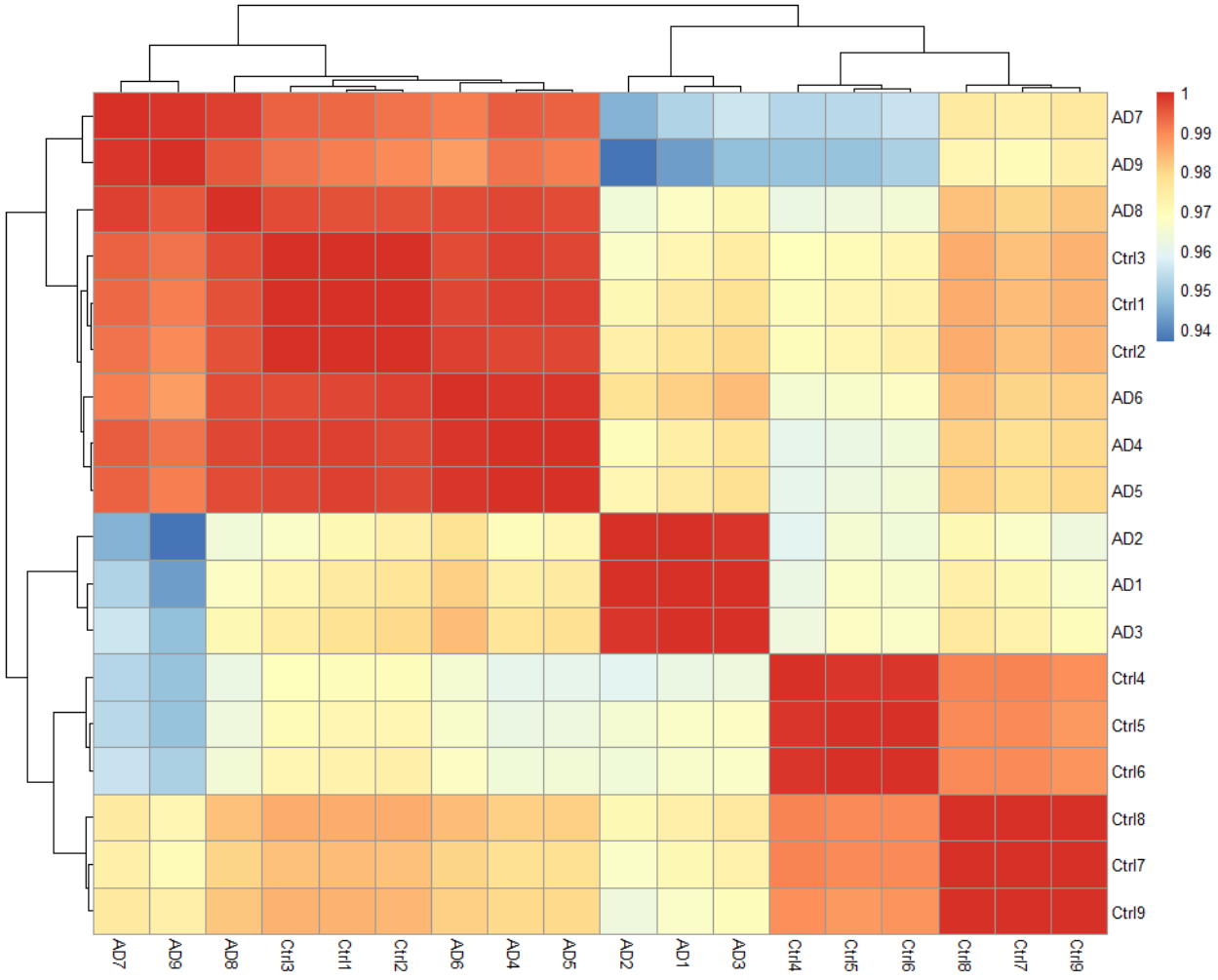

Figure 6: Heatmap and hierarchical clustering of differentially expressed genes from all samples generated from DeSeq2 data.

Analyzing potential functions of differential gene expression

All genes with greater than twofold upregulation and p-value of <0.05 were uploaded to String-DB for analysis of interactions between gene products (von Mering et al. 2005). K-means clustering was performed on the network and three distinct hubs were identified via interactions from curated databases and experimentally determined interactions. In the first cluster (green, left, Figure 7), the central gene/protein of interest is IL1β, implicated in multiple prior studies with inflammation, AD, and the immune response (Kinney et al. 2018). Closely tied to it are

genes from the Wnt pathway (Wnt5a), genes for differentiation (PDGFRA, platelet-derived growth factor receptor alpha), genes for second-messenger signaling pathways (ADCY6, adenylate cyclase type six), and closely related inflammation and cytokine/chemokine pathways (CXC family genes). The CXC genes act as pro-inflammatory signals, regulating the inflammation response that is particularly of note in AD as it has been shown in AD patient brains (Liu et al. 2014). Also upregulated was VCAM1, a proliferation marker, and IGF1R, insulin-related growth factor 1 receptor. Upregulation of this cluster, with a p-value of <0.05, as seen in this analysis strongly continues to support the theory that inflammation plays a role in the progression and severity of symptoms for AD at a molecular level.

The second cluster of note is closely related to the inflammation cluster seen by the cytokine/chemokine pathways, centering on genes of the complement system, which include C3, C5, CFB, C4a and C4b. The complement system (or complement cascade) regulates the immune response; this ties in closely with the upregulation of pro-inflammatory genes and cytokine/chemokine pathways. Importantly, the complement system is directly involved in synapse pruning and has been implicated in AD (Brucato 2020). Additionally, genes from the Ras-Raf-MEK-ERK signaling pathway are closely linked to the complement system gene cluster in this visualization and were upregulated in our dataset.

The last cluster of interest in blue included voltage-gated potassium channels and their subunits (KCNB1 family) and metalloproteases (ADAMTS1 family). Oxidation of KCNB1 channels has been reported in a mouse model of AD, which becomes toxic to neurons (Wei, Shin, and Sesti 2018). The ADAMTS1 family is associated with extracellular matrix damage and repair, and has been shown to be downregulated in animal models of neurodegenerative diseases such as multiple sclerosis (Gurses et al. 2016). There are also extracellular matrix gene linkages

and ion channels in the third cluster. Extracellular matrix protein levels have been shown to be changed in AD patients and animal models, and have been shown to interact with Aβ peptides (Ma et al. 2020).

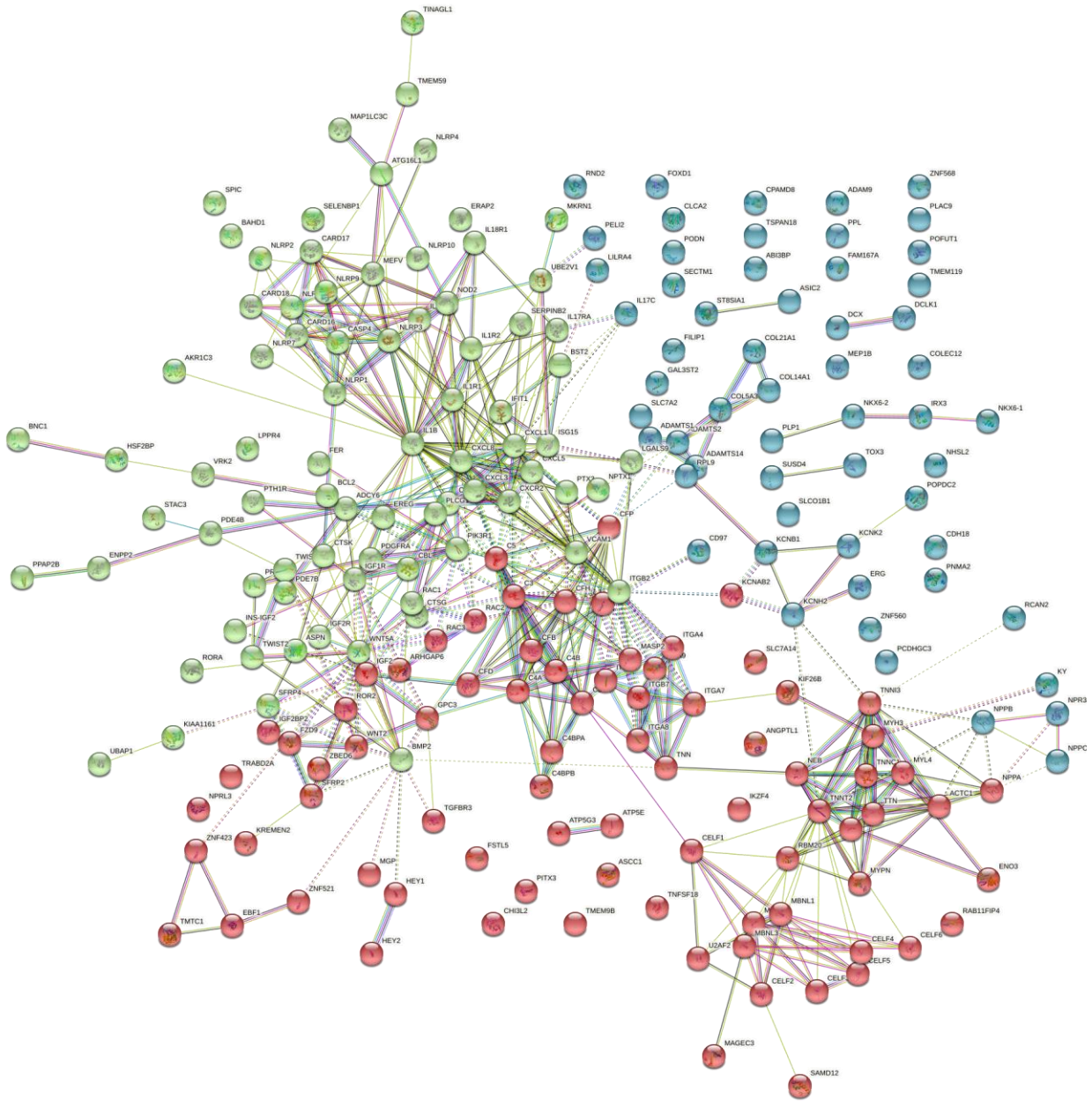

Figure 7: String-DB K-means clustering of differentially expressed genes ($p<0.05$), showing linked gene ontologies and gene families.

Functional interaction enrichments for biological process, molecular function, and cellular component gene ontology were analyzed from the DEGs in the String-DB generated network. DEGs and their associations with cell component gene ontology revealed connections to AD and inflammation with a high confidence score (Figure 8) (Szklarczyk et al. 2019). “Size” along the x-axis indicates a ranking of confidence, with 1 being the highest possible confidence (von Mering et al. 2005). The dot “strength” indicates strength of co-expression between the DEG list and the gene ontology term. Gene ontology analysis of the most upregulated DEGs were associated with terms for the integrin alpha4-beta7 complex, which is involved in the CD4 cell-surface complex formation to regulate the immune response, and surprisingly, the cardiac troponin complex (Cicala et al. 2009). Other upregulated cell components to note were the NLRP3 inflammasome complex, and inflammasome complex, and integrin complex, which are all involved with inflammation and the immune response.

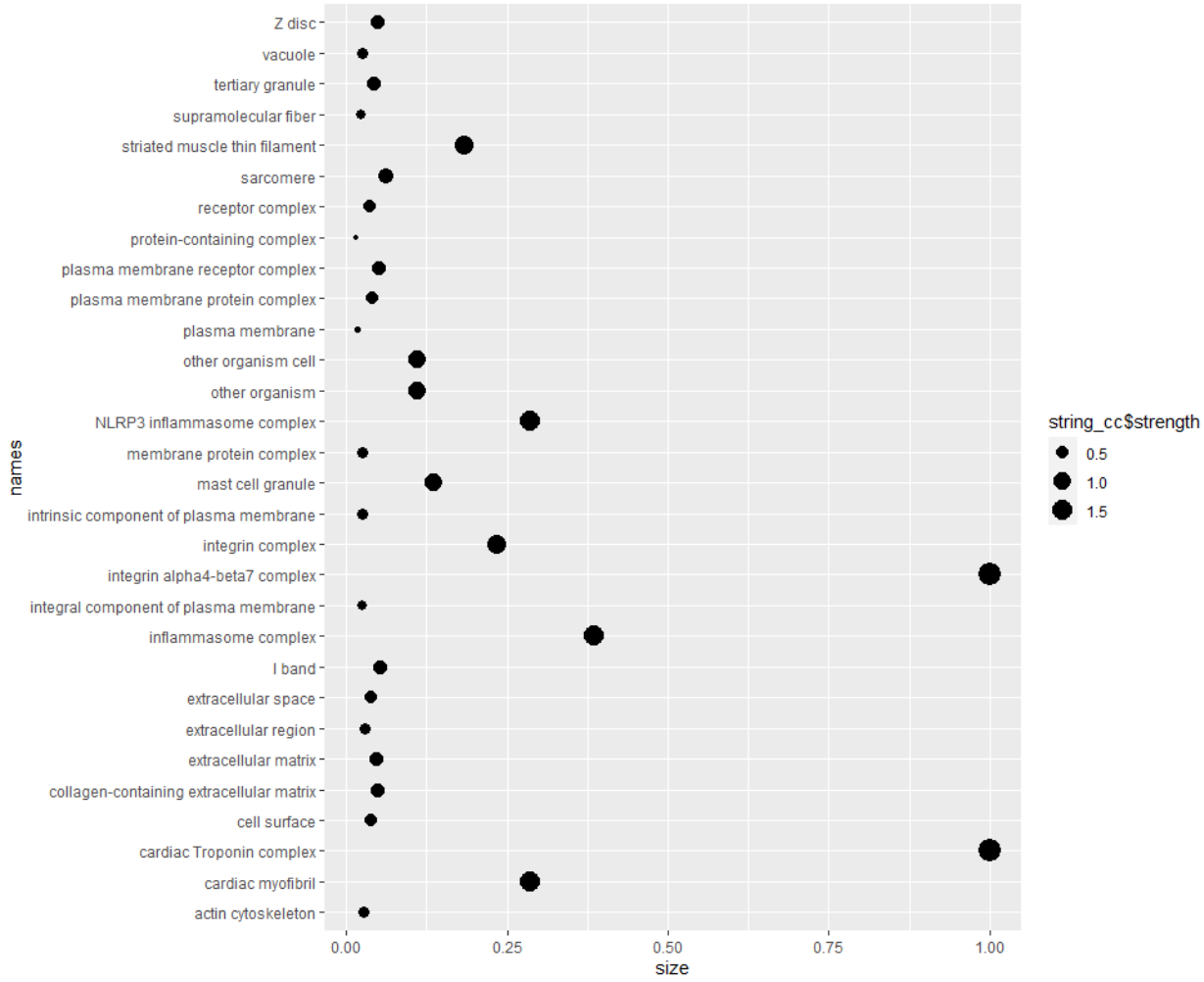

Figure 8: Cell component associations from differentially expressed genes from String-DB analysis.

The upregulated genes revealed patterns in upregulated gene processes as well, with regulation of cell proliferation in midbrain, the cell-matrix adhesion involved in amoeboid cell migration, cytokine secretion involved in immune response, and negative regulation of

complement activation significantly upregulated (Figure 9).

Figure 9: Top 30 gene processes associated with differentially expressed gene list generated by String-DB.

From the upregulated genes, molecular function associations yielded several functions of interest, including upregulation in microsatellite binding, multiple troponin binding types, insulin receptor binding, insulin binding, and insulin-like growth factor-activated receptor activity (Figure 10). This is consistent with previous research showing a change in metabolism by AD astrocytes: AD astrocytes have been previously shown to have impaired glycolytic flux (Le Douce et al. 2020)

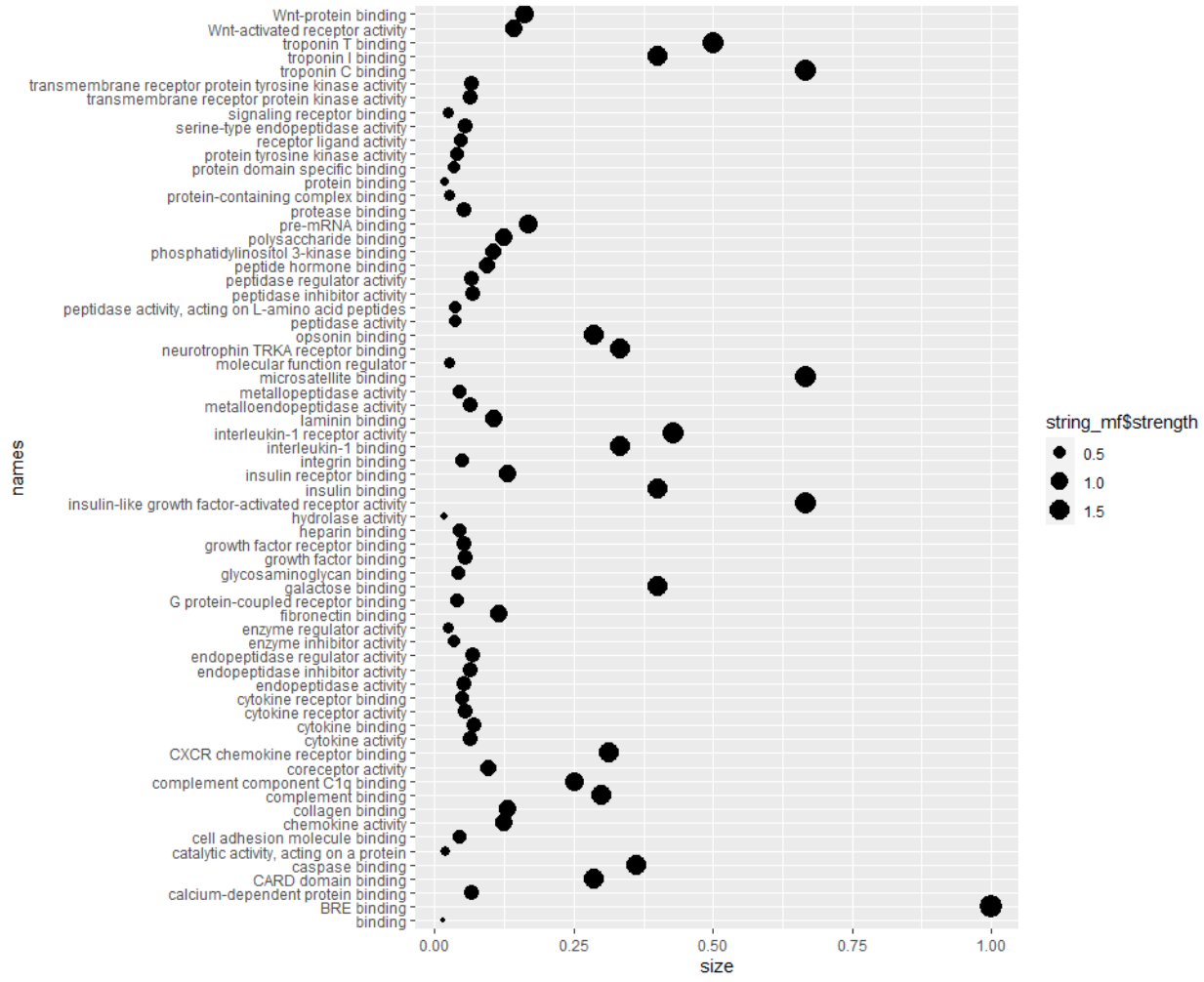

Figure 10: Molecular function associations for all differentially expressed genes generated by String-DB.

Gene Ontology Analysis

A more stringent analysis was performed on DEGs, that included only genes with a log two-fold change of great than 2 (up or down) and a p-value of less than or equal to 0.05 as determined by DEseq2. This analysis resulted in a smaller list of significant genes with 101 upregulated DEGs 169 downregulated DEGs. These up and downregulated genes were submitted to Enrichr and gene ontology analysis for biological function, molecular function, and cell component were performed (Figure 11). Of the upregulated genes, the most notable associated biological processes were related to inflammation (neutrophil chemotaxis, neutrophil migration,

granulocyte chemotaxis); unexpectedly, multiple processes involving muscle filament sliding and contraction were also upregulated. Of the molecular functions of the upregulated genes, a similar pattern formed with upregulation of chemokine receptor binding, chemokine activity, and cytokine activity as the top GO terms. Secondary to those molecular functions were related to actin binding, metallopeptidase activity, collagen binding, and actin filament binding. Lastly, the upregulated genes were associated with plasma membrane and actin cytoskeleton portions of the cell, as well as endoplasmic reticulum lumen. These upregulated genes point to increased motility of the AD astrocytes as well as increased cytokine secretion and inflammatory signalling.

Of the differentially downregulated genes, the top gene ontology terms for biological processes included cell-cell adhesion, cell morphogenesis, and various terms involving muscle morphogenesis and development. Of note are downregulation in processes for cell-cell junction organization, regulation of MAPK cascade, and positive regulation of cell communication: these support prior research indicating decreased cell signalling capability in AD astrocytes (Brambilla, Martorana, and Rossi 2013). The GO terms enriched in the downregulated genes for molecular function included multiple downstream secondary messenger pathways, GABA receptor activity, growth factor activity, and cytokine activity. Of the downregulated genes, the cell components which they were associated with were also portions of the plasma membrane, as well as the GABA-A receptor complex, vesicle membranes, and the early endosome membrane. The differential downregulation in the GABA receptor complex and activity continues to contribute to the pattern of decreased signalling capability in AD astrocytes (Rissman, De Blas, and Armstrong 2007).

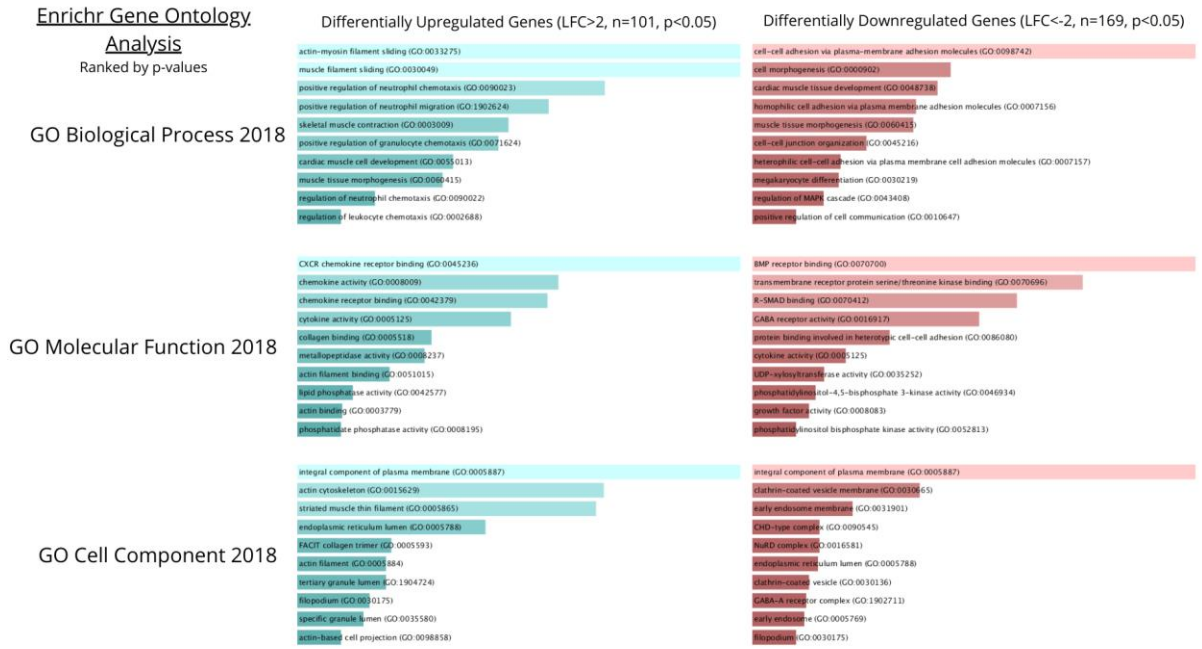

Figure 11: Gene ontologies for all differentially upregulated (n=101) and downregulated (n=169) ($p<0.05$) genes from Enrichr analysis ranked by p-values.

Differentially regulated ($p<0.05$) genes (both up- and downregulated) were also compared to existing gene libraries (Figure 12). These gene lists were Alzheimer Disease, Early Onset from DisGeNET (115 genes), Alzheimer Disease, Late Onset from DisGeNET (252 genes), Familial Alzheimer Disease (FAD) from DisGeNET (187 genes), and Inflammation mediated by chemokine and cytokine signaling pathway Homo sapiens P00031 from Panther_2016 (188 genes). Of the total number of genes which make up these categories, DEGs from our dataset accounted for the majority (>60%) of each category with $p<0.05$. The gene library with the highest percent of matches was from the familial AD library (140/187 genes present, 74.8% match), followed by early-onset (78/115, 67.8% match), late-onset (164/252, 65.0% match), and inflammation (115/188, 61.1% match) libraries. This continues to support the relationship between familial AD and early-onset AD, with literature-reported genes of interest PSEN1 (up), ApoE (down), Il1β (up) all differentially regulated between the AD and Ctrl

datasets. The differential regulation of inflammation-related genes continues to be supported by this data. It is unusual to see the downregulation of ApoE in this case as it is usually a risk factor for AD, but one study reported a heterozygous ApoE mutation conferred protection against the PSEN1 mutation and delayed early-onset AD in the patient (Zalocusky, Nelson, and Huang 2019)

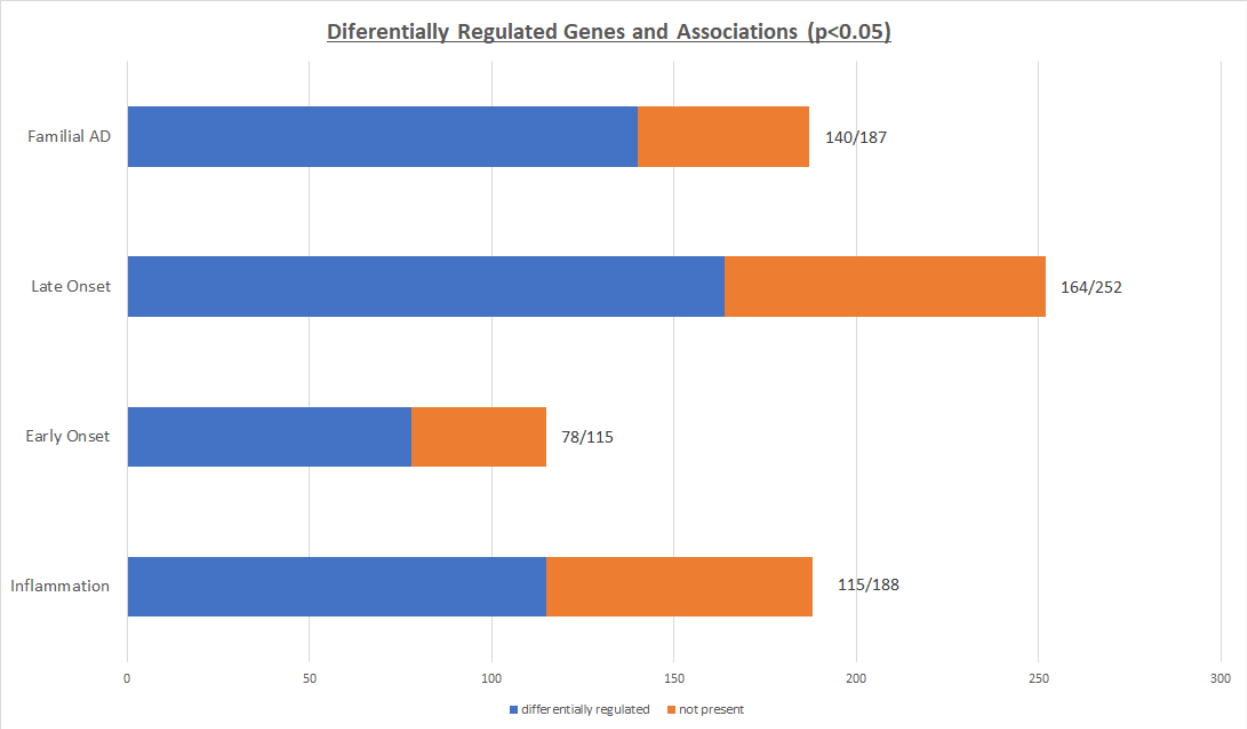

Figure 12: Differentially expressed genes compared to existing gene libraries for familial AD, early-onset, late-onset, and inflammation showing >60% present in the astrocyte samples.

Lastly, the DEGs were analyzed with respect to reported A1 and A2 upregulated genes from literature (Li et al. 2019) (Figure 13). Of the differentially expressed genes, 7/13 were upregulated, 4/13 were downregulated, and 2/13 were not present from the A2-associated gene group. Of the A1-associated genes, 4/12 were upregulated in our gene set, 2/12 were downregulated, and 6/12 were not significantly differentially expressed in our dataset. From this data, it is surprising to see that the AD astrocytes more closely resembled the A2 astrocytes than A1 astrocytes.

Though there were significant upregulated genes related to inflammation and astrogliosis, the astrocytes more closely resembled the A2 state as they had more commonly expressed DEGs, suggesting that neuroinflammation may be pushing the astrocytes to a more anti-inflammatory state, rather than further contributing to the inflammation response. This may further support the theory that neuroinflammation is facilitated by and caused by microglia rather than astrocytes (Hemonnot et al. 2019). This is significantly different from the initial hypothesis and though it points to a role of inflammation in astrocytes, the astrocytes may be responding by building a more robust anti-inflammatory response to repair the damage, encourage synaptic growth and neuronal survival, rather than contributing further to the pro-inflammatory response. This also suggests that A1 and A2 states are not so clearly defined and may fall along a spectrum of states rather than strict classifications; more research is required to confirm this (Liddelow 2017).

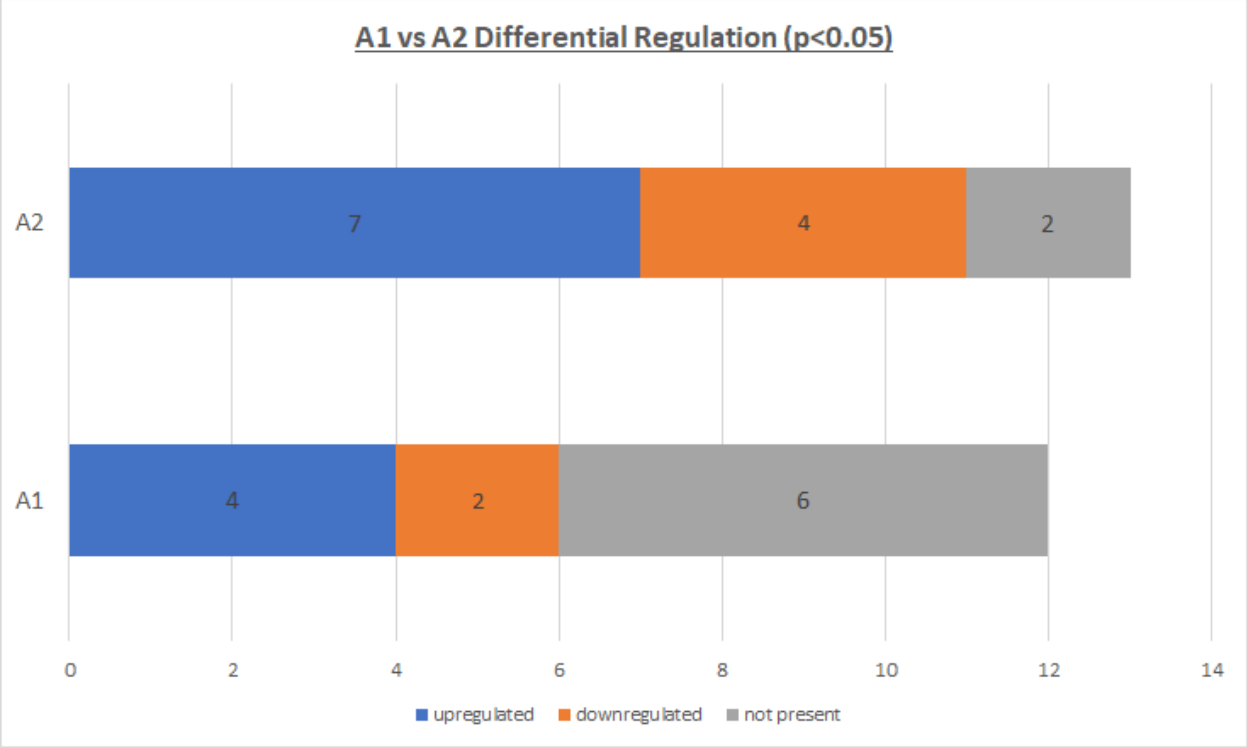

Figure 13: Differentially expressed (p<0.05) genes from the astrocyte dataset associated with A1 and A2 states. *Actual gene identifiers, log2FC, p-values and p-adjusted values of up/downregulation from A1 & A2 in supp. table 1.

DISCUSSION & FUTURE DIRECTIONS

The results of this study are consistent with previous literature illustrating neuroinflammation in AD, with significant changes in gene expression ($p<0.05$, LogFC>2) in pro-inflammatory, cell-signaling, and immune-related genes in AD astrocytes compared to controls (Kinney et al. 2018). This has not been demonstrated before in AD astrocytes, and suggests that the transcriptome of AD astrocytes is distinctly different from that of controls, which provides new insight into clinical applications for earlier detection of AD. It is also significant because our AD astrocytes were not previously exposed to neurons, suggesting these changes are attributable to the disease state. Though the data set displayed significant upregulation in inflammatory gene ontology (61.1% differentially expressed in our data set), we cannot conclude that the inflammation can be solely attributed to astrocytes, and the lack of co-culture with microglia or neurons in this experiment limits the conclusions that can be drawn about the feed-forward inflammation pattern hypothesized of AD.

The astrocytes in this study more closely resembled A2 astrocytes with 11/13 of the genes differentially expressed, compared to 6/12 of the A1 astrocyte genes. Previous studies showed that activated microglia were responsible for inducing the neurotoxic A1 state (Liddelow et al. 2017). In the absence of these activated microglia and without previous exposure to neurons, AD astrocytes more closely resembled the A2 state. However, these results may be different in astrocytes co-cultured with neurons or microglia, which is a future direction of interest.

It is also important to note the significant upregulation (LogFC = 3.182918) in C3 in the AD astrocytes compared to control, which is the most significant A1 “marker”. Its A2 counterpart, S100a10, was only upregulated with LogFC = 0.142075 (Supp. Table 1). However,

other A2-associated genes such as Ptx3 (LogFC = 2.359031) and Emp1 (LogFC = 1.191145) were significantly upregulated, and are tied to A2 roles that activate the complement cascade, signaling, and proliferation. The significant upregulation in C3 may be tied to an overall increase in pro-inflammatory genes associated with AD rather than only being attributed to a neurotoxic A1 state. AMIGO2, an A1-associated gene, was also significantly downregulated (LogFC = -2.47877) when it was expected to be upregulated (Li et al. 2019).

Out of the significant differentially regulated genes, the AD genes more closely resembled the familial AD library (140/187 genes present, 74.8% match) and early-onset library (78/115, 67.8% match) rather than the late-onset library (164/252, 65.0% match). This finding may more reflect the state of the literature more than the biology of our astrocytes as almost all published databases are derived from familial lines, whereas our astrocytes were derived from sporadic AD patients. Alternatively, this point may suggest a closer correlation between familial AD genes and sporadic AD, which may be useful for prediction and detection of AD. Literature has also suggested that epigenetic mechanisms may play an essential role in disease development that may differ between sporadic and familial forms: more research is needed to conclude this (Piaceri, Nacmias, and Sorbi 2013). As ~85% of AD cases are of the sporadic type, it is imperative that the field continues its research in this area to identify potential treatments, prevention methods, and early-detection methods for sporadic AD (Awada 2015).

SUPPLEMENTAL FIGURES

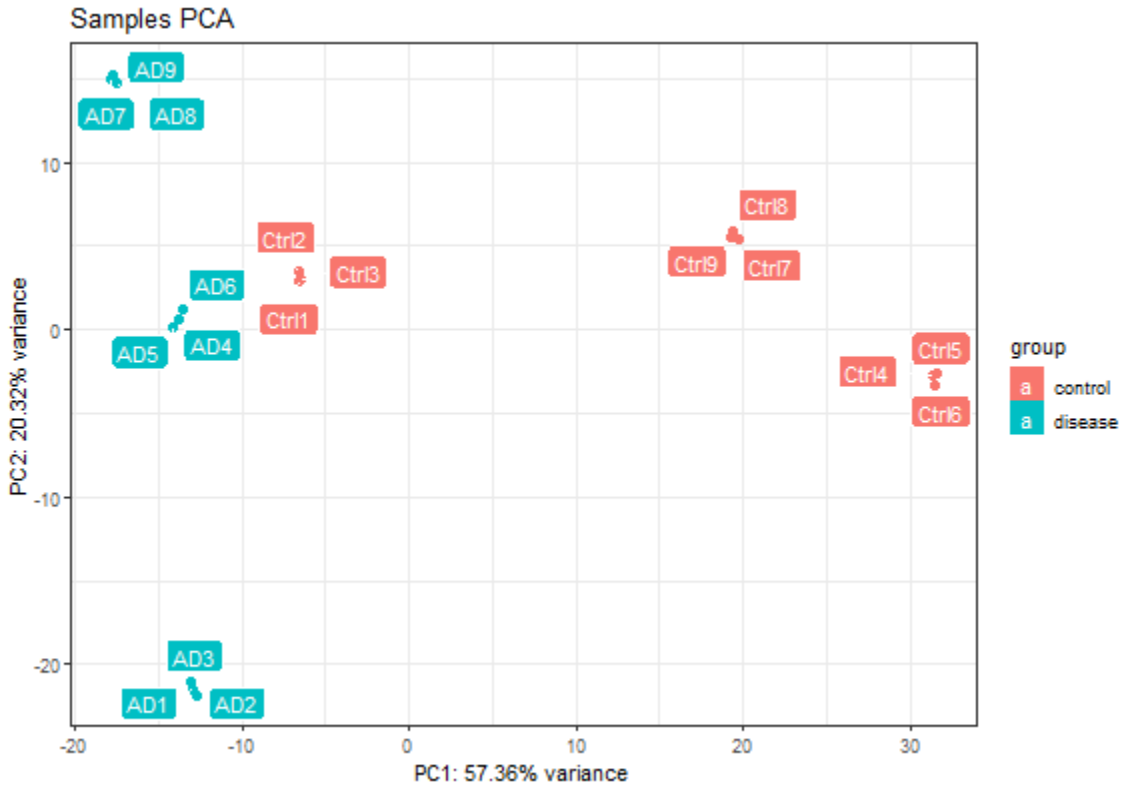

Supplemental Figure 1: Principal component analysis with individual sample identifications, clustered by group AD vs control, generated with pcaExplorer (Marini and Binder 2019).

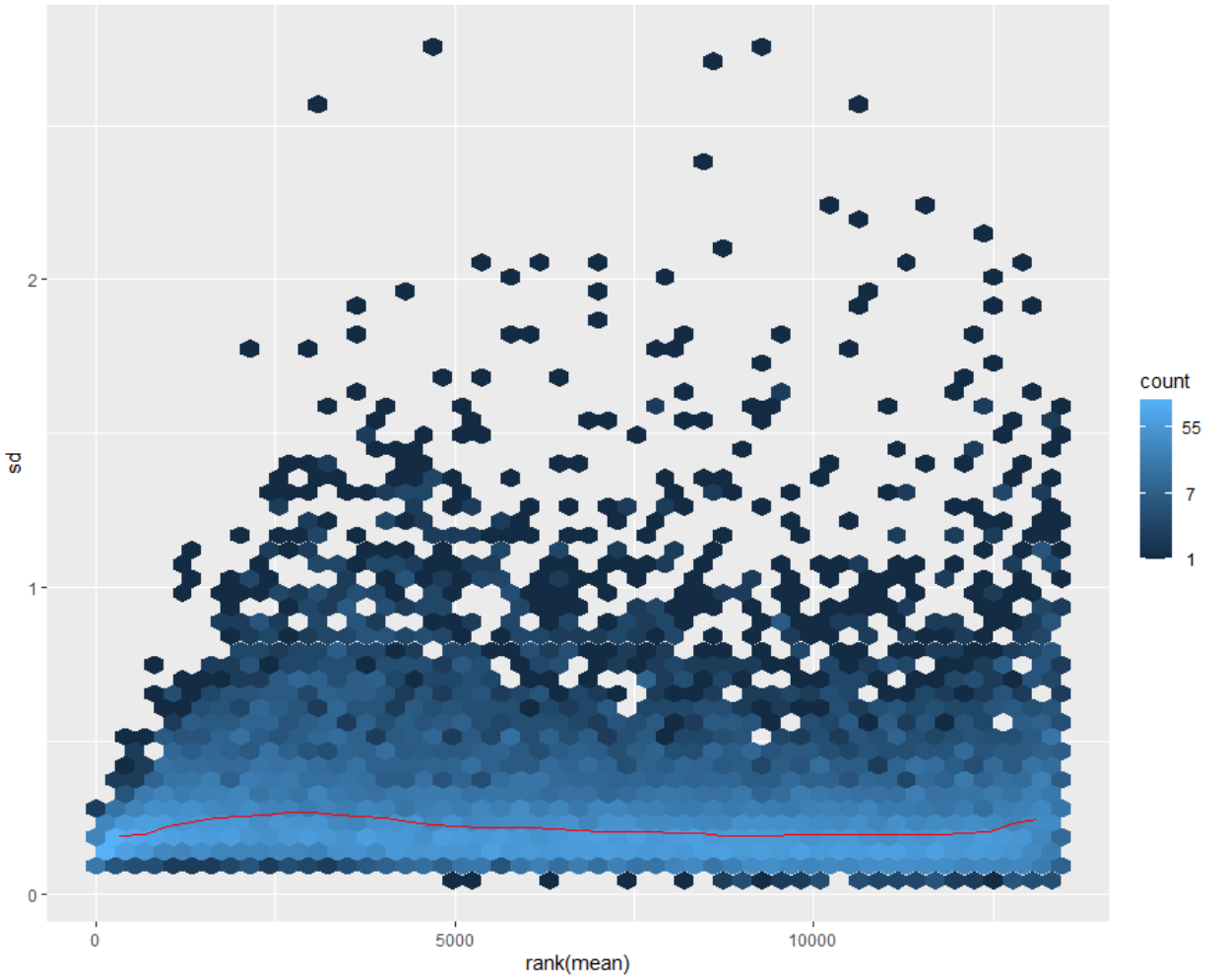

Supplemental Figure 2: Variance Stabilizing Transformation (VST) of dataset, used in DeSeq2 analysis.

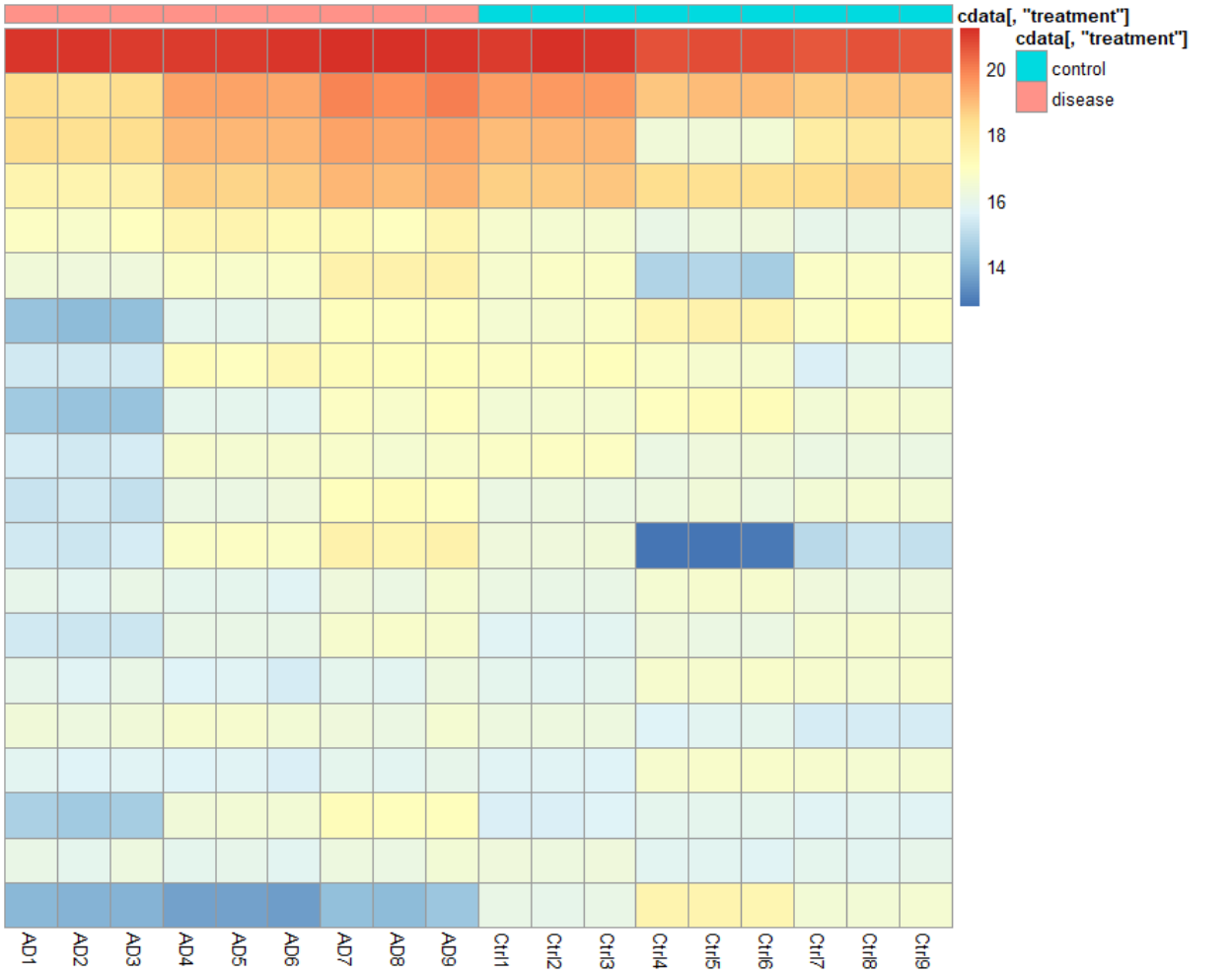

Supplemental Figure 3: Heatmap generated from variance stabilizing transformed data illustrating biased clustering. There is less variation in this heatmap than Figure 3 likely due to the normalization.

Supplemental Table 1: A1 and A2 genes and log2FoldChange, p-value, and p-adjusted values from this dataset. All values $p<0.05$. n.p. = not present

A1	**log2FoldChange**	**pvalue**	**padj**
H2-D1	n.p.		
IIGP1	n.p.		
PSMB8	n.p.		
SRGN	0.322346	0.417637	0.598837
AMIGO2	-2.47877	1.63E-21	6.09E-19
SERPING1	0.595193	0.151633	0.304989
GGTA1	n.p.		
HW-T23	n.p.		
GPP2	n.p.		
FKBP5	-0.00577	0.977321	0.98821
C3	3.182918	2.43E-05	0.000312
FBLN5	0.831142	0.006555	0.029155
A2	**log2FoldChange**	**pvalue**	**padj**
Clcf1	-0.84991	0.000109	0.001071
Tgm1	0.963734	0.011254	0.044171
Ptx3	2.359031	3.36E-05	0.00041
S100a10	0.142075	0.530744	0.694614
Sphk1	-0.53995	0.005019	0.023479
Cd109	-0.55917	2.28E-10	1.29E-08
Ptgs2	-0.03986	0.821882	0.898261
Emp1	1.191145	7.37E-05	0.000769
Slc10a6	n.p.		
Tm4sf1	0.310014	0.097334	0.222444

Supplemental Table 1: A1 and A2 genes and log2FoldChange, p-value, and p-adjusted values from this dataset. All values p<0.05. n.p. = not present, continued			
A2	**log2FoldChange**	**pvalue**	**padj**
B3gnt5	0.138028	0.485333	0.656777
Cd14	n.p.		
Stat3	0.294854	3.59E-05	0.000433

Supplemental Table 2: Differentially upregulated genes and log2FoldChange, p-value, and p-adjusted values from this dataset. All values p<0.05.

Upregulated Genes	**log2FoldChange**	**pvalue**	**padj**
ABI3BP	2.685213	0.000245	0.002055
ACTC1	4.915088	8.15E-05	0.000838
ADAMTS1	2.038403	1.30E-16	2.69E-14
ADAMTS2	2.681236	1.37E-05	0.000195
ADGRE5	2.37332	1.53E-12	1.40E-10
ANGPTL1	2.11516	0.000991	0.006453
ARHGAP6	2.564953	1.37E-09	6.38E-08
ASPN	4.00088	3.82E-11	2.62E-09
ATP5F1E	2.165929	1.67E-05	0.000229
BNC1	2.024166	9.53E-05	0.000956
BST2	2.137641	3.13E-08	9.93E-07
C3	3.182918	2.43E-05	0.000312
CDH18	2.815228	1.64E-06	3.22E-05
CHI3L2	2.514101	0.000178	0.001582
CLCA2	2.437934	0.001884	0.01079
COL14A1	2.628606	8.53E-07	1.82E-05
COL21A1	4.635872	3.60E-09	1.48E-07

Supplemental Table 2: Differentially upregulated genes and log2FoldChange, p-value, and p-adjusted values from this dataset. All values p<0.05, continued.

Upregulated Genes	log2FoldChange	pvalue	padj
COL5A3	2.156682	0.001583	0.0094
COLEC12	2.586665	9.29E-18	2.23E-15
CTSK	3.763913	1.21E-31	1.09E-28
CXCL1	4.213759	2.61E-12	2.25E-10
CXCL3	2.828405	1.88E-12	1.65E-10
CXCL5	3.019072	1.94E-07	4.94E-06
CXCL6	3.393492	3.29E-10	1.81E-08
CXCL8	2.892556	5.14E-07	1.17E-05
DCLK1	2.493678	1.28E-06	2.58E-05
EBF1	2.039797	6.80E-11	4.34E-09
ELN	2.476029	0.028118	0.088948
ENO3	3.317624	2.76E-07	6.72E-06
ENPP2	2.525136	9.59E-12	7.41E-10
ERAP2	2.719549	2.45E-08	8.13E-07
EREG	2.4048	8.00E-07	1.72E-05
ERG	3.384284	5.57E-05	0.000613
FAM167A	2.127629	7.65E-05	0.000794
FILIP1	2.449946	0.00014	0.0013
FSTL5	3.797814	5.61E-07	1.27E-05
HEY2	2.552646	8.69E-05	0.000884
IFIT1	2.258584	2.37E-13	2.59E-11
IGF2	4.343556	1.52E-10	9.16E-09
IL1B	3.4109	2.99E-06	5.45E-05

Supplemental Table 2: Differentially upregulated genes and log2FoldChange, p-value, and p-adjusted values from this dataset. All values p<0.05, continued.

Upregulated Genes	log2FoldChange	pvalue	padj
IRX3	2.273251	2.90E-14	3.72E-12
ITGA7	2.457062	4.52E-10	2.36E-08
ITGA8	2.523243	0.00581	0.026401
KCNB1	2.230243	0.000114	0.001099
KCNK2	3.200713	2.93E-11	2.03E-09
KREMEN2	2.296043	0.002641	0.014139
KY	2.33402	2.41E-06	4.51E-05
LINC00869	2.402602	1.34E-11	9.88E-10
LOC730101	2.102725	9.81E-11	6.11E-09
MAP1LC3C	2.295673	1.04E-07	2.86E-06
MGP	3.657555	2.32E-37	4.46E-34
MYH3	7.428292	1.60E-10	9.54E-09
MYL4	3.126259	1.18E-05	0.000173
MYPN	2.220905	4.27E-05	0.000498
NEB	3.800056	9.93E-05	0.000987
NHSL2	2.292378	4.15E-11	2.83E-09
NPR3	2.114785	0.000292	0.002373
NPTX1	3.428522	6.45E-15	9.86E-13
PDE4B	2.024184	1.82E-12	1.62E-10
PDE7B	3.054406	1.63E-07	4.23E-06
PDGFRA	2.498424	0.000211	0.001826
PLAC9	2.159798	1.34E-07	3.59E-06
PLP1	2.045277	1.44E-14	2.00E-12

Supplemental Table 2: Differentially upregulated genes and log2FoldChange, p-value, and p-adjusted values from this dataset. All values p<0.05, continued.

Upregulated Genes	log2FoldChange	pvalue	padj
PLPP3	2.128656	0.000113	0.001095
PLPPR4	2.986062	4.28E-06	7.40E-05
PNMA2	2.060199	0.000847	0.005687
PODN	2.24589	1.81E-05	0.000245
PPL	2.508454	8.41E-07	1.80E-05
PRDM16-DT	2.06191	9.50E-08	2.63E-06
PRRX1	2.466145	1.70E-10	1.01E-08
PTH1R	2.741176	3.46E-05	0.000419
PTX3	2.359031	3.36E-05	0.00041
RAB11FIP4	3.19363	4.14E-16	8.07E-14
RCAN2	2.105669	1.62E-05	0.000224
RELN	2.11747	0.025164	0.081955
ROR2	2.818234	8.97E-08	2.50E-06
RPL9	3.358643	4.82E-12	3.95E-10
SAMD12	2.070903	2.62E-07	6.41E-06
SECTM1	4.498976	4.22E-81	5.68E-77
SELENBP1	2.680398	2.59E-08	8.52E-07
SERPINB2	3.243222	2.19E-11	1.56E-09
SFRP2	4.983	6.51E-08	1.89E-06
SFRP4	2.002569	0.004248	0.020558
SFTA1P	2.597378	4.41E-09	1.78E-07
SLC7A14	2.35032	0.000174	0.001553
SLC7A2	3.151247	7.56E-15	1.13E-12

Supplemental Table 2: Differentially upregulated genes and log2FoldChange, p-value, and p-adjusted values from this dataset. All values p<0.05, continued.

Upregulated Genes	**log2FoldChange**	**pvalue**	**padj**
ST8SIA1	2.107076	1.55E-09	7.10E-08
STAC3	3.951911	7.78E-07	1.68E-05
TGFBR3	2.590984	6.06E-29	4.80E-26
TINAGL1	2.452342	0.000288	0.002347
TMEM119	3.008593	0.000113	0.001095
TMTC1	2.257303	2.36E-08	7.87E-07
TNNC1	3.12855	5.61E-05	0.000616
TNNT2	5.956004	1.77E-08	6.12E-07
TRABD2A	2.294568	1.76E-05	0.00024
TSPAN18	2.363879	0.001132	0.007166
TTN	2.362393	4.08E-06	7.11E-05
VCAM1	2.606968	0.003743	0.018644
WNT2	3.485474	9.19E-10	4.43E-08
ZNF528-AS1	2.185297	1.66E-15	2.94E-13
ZNF560	2.235274	2.45E-06	4.57E-05

Supplemental Table 3: Differentially downregulated genes and log2FoldChange, p-value, and p-adjusted values from this dataset. All values p<0.05.

Downregulated Genes	**log2FoldChange**	**pvalue**	**padj**
ACTBL2	-2.52666	1.60E-17	3.70E-15
ACTG2	-2.25957	7.03E-11	4.44E-09
ACVR1C	-2.92695	1.56E-05	0.000217
ADAMTS16	-2.91692	7.31E-07	1.59E-05

Supplemental Table 3: Differentially downregulated genes and log2FoldChange, p-value, and p-adjusted values from this dataset. All values p<0.05, continued.

Downregulated Genes	log2FoldChange	pvalue	padj
ADAMTS9	-2.67483	5.71E-05	0.000623
ADGRL3	-2.62219	0.00184	0.010598
ALDH1A3	-2.49886	0.000174	0.001551
AMIGO2	-2.47877	1.63E-21	6.09E-19
ANKRD1	-3.26576	5.99E-22	2.44E-19
ANO4	-4.58202	9.59E-10	4.61E-08
ANOS1	-2.36696	2.60E-05	0.000331
AQP1	-2.12013	0.000125	0.001186
ARAP2	-2.12721	4.78E-07	1.10E-05
B3GALT5	-2.22809	2.85E-06	5.23E-05
B3GALT5-AS1	-2.05547	1.53E-05	0.000214
B4GALNT1	-2.56173	2.85E-07	6.93E-06
BAALC	-2.76473	5.43E-08	1.62E-06
BACH2	-2.18916	5.79E-12	4.67E-10
BCHE	-2.73752	2.52E-44	6.79E-41
BEGAIN	-2.66411	1.01E-05	0.000152
BMP2	-2.40422	9.10E-10	4.42E-08
BMP4	-3.03396	8.43E-09	3.12E-07
BMP6	-2.71906	6.81E-08	1.96E-06
BTBD11	-2.63132	3.90E-06	6.87E-05
C5orf46	-2.50126	4.95E-25	2.56E-22
CACNA2D3	-2.40994	0.001027	0.006633

Supplemental Table 3: Differentially downregulated genes and log2FoldChange, p-value, and p-adjusted values from this dataset. All values p<0.05, continued.

Downregulated Genes	**log2FoldChange**	**pvalue**	**padj**
CACNG4	-3.60728	2.59E-08	8.52E-07
CADM1	-3.81757	1.06E-20	3.49E-18
CADM3	-4.01514	5.75E-05	0.000625
CCDC81	-2.32226	2.16E-11	1.54E-09
CD24	-3.22019	1.95E-23	9.05E-21
CDH10	-2.46638	1.49E-10	9.04E-09
CDH6	-2.07441	7.68E-05	0.000797
CDKN2B	-2.68322	5.50E-20	1.72E-17
CELSR1	-3.13868	7.15E-12	5.63E-10
CHD5	-2.0722	1.32E-05	0.00019
CHRM2	-3.80955	6.25E-12	4.97E-10
CLSTN2	-2.52946	7.83E-09	2.93E-07
CNTNAP3	-3.40524	2.09E-19	6.12E-17
COL11A1	-3.3353	6.70E-11	4.31E-09
COL25A1	-4.55126	1.78E-35	2.39E-32
COL7A1	-2.00872	0.000165	0.001492
CXADR	-2.3936	1.03E-06	2.13E-05
DACH1	-3.13273	3.84E-10	2.08E-08
DCBLD1	-2.34442	4.56E-14	5.58E-12
DCLK2	-2.47053	7.50E-13	7.37E-11
DIRAS3	-2.21371	0.000537	0.003908
DOK6	-3.94813	8.02E-13	7.82E-11

Supplemental Table 3: Differentially downregulated genes and log2FoldChange, p-value, and p-adjusted values from this dataset. All values p<0.05, continued.

Downregulated Genes	**log2FoldChange**	**pvalue**	**padj**
DSC3	-2.34503	1.37E-05	0.000195
DSG2	-2.18938	5.42E-16	1.03E-13
DYNC1I1	-3.67947	8.72E-09	3.21E-07
EDN1	-2.44488	8.57E-25	4.27E-22
EGF	-2.44351	1.96E-06	3.80E-05
EPHA3	-2.02705	8.66E-07	1.84E-05
EPHA4	-2.45358	4.99E-11	3.36E-09
ERMN	-4.99101	4.36E-12	3.65E-10
FAM198B-AS1	-2.17181	4.00E-07	9.29E-06
FAT3	-2.501	2.21E-07	5.56E-06
FLJ16779	-4.91521	2.14E-10	1.23E-08
FSTL3	-2.35005	6.05E-10	3.06E-08
GABBR2	-2.22742	2.74E-07	6.69E-06
GABRA5	-3.68904	3.45E-06	6.21E-05
GABRB3	-2.44738	0.000217	0.001868
GASK1B	-2.07925	2.84E-11	1.99E-09
GNA14	-2.05097	8.60E-05	0.000875
GPAT3	-2.07235	9.08E-07	1.92E-05
GPC4	-3.68079	8.19E-09	3.03E-07
GREM2	-2.15449	5.80E-05	0.00063
GRIP1	-2.02287	0.000214	0.001845
HOXB2	-3.4419	9.22E-09	3.36E-07

Supplemental Table 3: Differentially downregulated genes and log2FoldChange, p-value, and p-adjusted values from this dataset. All values p<0.05, continued.

Downregulated Genes	**log2FoldChange**	**pvalue**	**padj**
HSD17B6	-3.07198	1.06E-08	3.81E-07
HSPB8	-2.03764	1.13E-09	5.35E-08
IGFBPL1	-2.50161	0.000319	0.002553
IGSF10	-2.49598	9.72E-08	2.69E-06
IL11	-2.37512	2.66E-08	8.72E-07
IL7R	-2.43884	9.95E-15	1.44E-12
INSYN2A	-2.02882	4.43E-05	0.000512
ITGB8	-2.10956	1.87E-08	6.39E-07
JAKMIP2	-2.22862	9.24E-05	0.000933
KCNH1	-2.15448	2.27E-08	7.60E-07
KCNJ2	-2.7627	1.25E-06	2.54E-05
KIF5A	-3.8533	1.94E-17	4.42E-15
KISS1	-4.15162	8.76E-14	1.04E-11
KIT	-2.52305	2.40E-05	0.000309
KRT7	-3.77202	1.49E-05	0.000209
LAMC2	-2.66003	1.88E-06	3.66E-05
LARGE1	-2.21855	8.28E-06	0.000127
LBH	-2.06319	2.02E-08	6.89E-07
LDLRAD4	-4.45603	1.70E-10	1.01E-08
LIMCH1	-2.00896	5.09E-05	0.00057
LINC00862	-3.29514	3.26E-07	7.78E-06
LINC01239	-2.09343	1.66E-09	7.56E-08

Supplemental Table 3: Differentially downregulated genes and log2FoldChange, p-value, and p-adjusted values from this dataset. All values p<0.05, continued.

Downregulated Genes	**log2FoldChange**	**pvalue**	**padj**
LIPG	-2.53351	8.63E-07	1.84E-05
LIPH	-2.91343	8.38E-06	0.000129
LOC101928595	-3.18134	0.00019	0.001671
LRATD2	-3.58517	2.17E-15	3.65E-13
LUZP2	-2.48735	2.83E-08	9.15E-07
LYPD1	-3.4772	1.27E-13	1.47E-11
LYPD6	-2.13936	5.69E-05	0.000622
MAGEL2	-2.85819	8.97E-13	8.62E-11
MAP3K9	-3.33963	2.14E-14	2.85E-12
MCTP1	-2.31895	2.20E-06	4.18E-05
MEIS1	-2.35233	2.82E-33	2.92E-30
MMP24	-2.3608	6.61E-05	0.000703
MYCT1	-4.72944	7.41E-32	7.12E-29
MYLK	-2.05452	4.25E-23	1.84E-20
MYLK2	-2.24093	5.05E-11	3.38E-09
MYOZ1	-2.1801	0.000334	0.002656
MYRF	-2.62536	3.62E-23	1.62E-20
NCF2	-2.87024	7.42E-13	7.35E-11
NKAIN4	-4.12496	4.61E-08	1.39E-06
NOVA2	-4.25467	2.66E-09	1.14E-07
NOX4	-2.14452	2.12E-08	7.19E-07
NPPB	-5.15645	2.53E-09	1.09E-07

Supplemental Table 3: Differentially downregulated genes and log2FoldChange, p-value, and p-adjusted values from this dataset. All values p<0.05, continued.

Downregulated Genes	**log2FoldChange**	**pvalue**	**padj**
NRG1	-2.45064	3.55E-13	3.73E-11
OTULINL	-2.22134	6.99E-09	2.68E-07
PALMD	-2.25866	1.93E-06	3.74E-05
PCDHGA2	-2.02935	0.006168	0.027755
PDE11A	-3.66665	1.85E-09	8.33E-08
PDGFB	-4.16758	5.50E-08	1.63E-06
PLPP4	-2.14715	9.63E-11	6.02E-09
PLPPR3	-2.13941	1.33E-05	0.000191
PLXDC1	-2.23861	6.26E-07	1.38E-05
PLXDC2	-2.83034	4.42E-12	3.65E-10
PMEPA1	-2.53538	1.40E-14	1.97E-12
PPP1R14A	-2.00451	8.55E-06	0.000131
PTPRE	-2.0262	6.86E-08	1.97E-06
PWWP3B	-2.43542	4.22E-05	0.000494
QPCT	-2.04045	5.94E-42	1.33E-38
RAC2	-2.21984	7.56E-05	0.000786
RASGRF2	-3.2767	1.54E-11	1.13E-09
RBP1	-4.18406	4.96E-12	4.02E-10
RIMS2	-2.65511	2.27E-07	5.69E-06
RPS28	-3.92513	9.63E-10	4.61E-08
RTN1	-4.46368	1.01E-10	6.24E-09
SALL1	-2.51743	1.08E-07	2.94E-06

Supplemental Table 3: Differentially downregulated genes and log2FoldChange, p-value, and p-adjusted values from this dataset. All values p<0.05, continued.

Downregulated Genes	**log2FoldChange**	**pvalue**	**padj**
SDC1	-2.23455	1.32E-05	0.00019
SHC4	-3.12482	1.40E-10	8.53E-09
SHROOM3	-2.04949	1.78E-13	2.01E-11
SIGLEC15	-2.00466	6.35E-11	4.13E-09
SLC15A4	-2.9534	4.95E-09	1.97E-07
SLC35F3	-3.59926	1.77E-07	4.58E-06
SLCO3A1	-2.95581	7.36E-09	2.80E-07
SNRPN	-2.01656	3.70E-06	6.57E-05
SORBS1	-2.11538	6.36E-06	0.000103
SORCS2	-2.38388	0.000127	0.001198
SOX5	-2.24511	2.73E-05	0.000344
SPINT2	-2.02041	4.60E-09	1.84E-07
SPP1	-3.99776	2.09E-13	2.31E-11
SPTBN2	-2.85316	5.16E-11	3.43E-09
ST8SIA6	-2.35005	9.13E-07	1.92E-05
SYNDIG1	-2.06605	0.002213	0.012236
SYT1	-2.40706	3.85E-08	1.18E-06
TAFA5	-2.29658	0.002803	0.014782
TAGLN3	-2.72439	0.000107	0.001052
TENM2	-4.4537	8.98E-08	2.50E-06
TGFBI	-2.74274	5.77E-37	9.70E-34
TLL2	-2.91693	1.03E-07	2.84E-06

Supplemental Table 3: Differentially downregulated genes and log2FoldChange, p-value, and p-adjusted values from this dataset. All values p<0.05, continued.

Downregulated Genes	**log2FoldChange**	**pvalue**	**padj**
TMEM35A	-2.17364	5.34E-15	8.26E-13
TNFAIP2	-2.83776	2.68E-15	4.45E-13
TNFSF4	-2.46034	2.28E-05	0.000296
TRPV2	-2.23202	0.01019	0.04105
TSPAN2	-3.18684	1.28E-06	2.58E-05
TYRP1	-2.34239	4.21E-05	0.000492
VAT1L	-2.87041	4.44E-05	0.000513
WNK4	-2.32157	4.92E-11	3.33E-09
XYLT1	-4.92837	6.43E-13	6.51E-11
ZFPM2	-2.65357	2.82E-13	3.06E-11
ZNF503	-2.19006	2.30E-14	3.00E-12

REFERENCES

Adler, C. H., Beach, T. G., Zhang, N., Shill, H. A., Driver-Dunckley, E., Caviness, J. N., Mehta, S. H., Sabbagh, M. N., Serrano, G. E., Sue, L. I., Belden, C. M., Powell, J., Jacobson, S. A., Zamrini, E., Shprecher, D., Davis, K. J., Dugger, B. N., & Hentz, J. G. (2019). Unified Staging System for Lewy Body Disorders: Clinicopathologic Correlations and Comparison to Braak Staging. *Journal of Neuropathology and Experimental Neurology*, *78*(10), 891–899.

Alzheimer's Disease Diagnostic Guidelines. (n.d.-a). Retrieved November 9, 2020, from http://www.nia.nih.gov/health/alzheimers-disease-diagnostic-guidelines

Anderson, M. A., Burda, J. E., Ren, Y., Ao, Y., O'Shea, T. M., Kawaguchi, R., Coppola, G., Khakh, B. S., Deming, T. J., & Sofroniew, M. V. (2016). Astrocyte scar formation aids central nervous system axon regeneration. *Nature*, *532*(7598), 195–200.

Awada, A. A. (2015). Early and late-onset Alzheimer's disease: What are the differences? *Journal of Neurosciences in Rural Practice*, *6*(3), 455.

Baik, S. H., Kang, S., Son, S. M., & Mook-Jung, I. (2016). Microglia contributes to plaque growth by cell death due to uptake of amyloid β in the brain of Alzheimer's disease mouse model. *Glia*, *64*(12), 2274–2290.

Bali, J., Gheinani, A. H., Zurbriggen, S., & Rajendran, L. (2012). Role of genes linked to sporadic Alzheimer's disease risk in the production of β-amyloid peptides. *Proceedings of the National Academy of Sciences of the United States of America*, *109*(38). https://doi.org/10.1073/pnas.1201632109

Brambilla, L., Martorana, F., & Rossi, D. (2013). Astrocyte signaling and neurodegeneration: New insights into CNS disorders. *Prion*, *7*(1), 28.

Chen, E. Y., Tan, C. M., Kou, Y., Duan, Q., Wang, Z., Meirelles, G. V., Clark, N. R., & Ma'ayan, A. (2013). Enrichr: interactive and collaborative HTML5 gene list enrichment analysis tool. *BMC Bioinformatics*, *14*(1), 1–14.

Chen, Y., Lun, A. T. L., & Smyth, G. K. (2016). From reads to genes to pathways: differential expression analysis of RNA-Seq experiments using Rsubread and the edgeR quasi-likelihood pipeline. *F1000Research*, *5*, 1438.

Cicala, C., Martinelli, E., McNally, J. P., Goode, D. J., Gopaul, R., Hiatt, J., Jelicic, K., Kottilil, S., Macleod, K., O'Shea, A., Patel, N., Van Ryk, D., Wei, D., Pascuccio, M., Yi, L., McKinnon, L., Izulla, P., Kimani, J., Kaul, R., … Arthos, J. (2009). The integrin alpha4beta7 forms a complex with cell-surface CD4 and defines a T-cell subset that is highly susceptible to infection by HIV-1. *Proceedings of the National Academy of Sciences of the United States of America*, *106*(49). https://doi.org/10.1073/pnas.0911796106

Clarke, L. E., Liddelow, S. A., Chakraborty, C., Münch, A. E., Heiman, M., & Barres, B. A. (2018). Normal aging induces A1-like astrocyte reactivity. *Proceedings of the National Academy of Sciences of the United States of America*, *115*(8), E1896–E1905.

Cummings, J. (2012). Alzheimer's disease diagnostic criteria: practical applications. *Alzheimer's Research & Therapy*, *4*(5), 35.

Dementia. (n.d.). Retrieved February 24, 2021, from https://www.who.int/news-room/fact-sheets/detail/dementia

Dobin, A., Davis, C. A., Schlesinger, F., Drenkow, J., Zaleski, C., Jha, S., Batut, P., Chaisson, M., & Gingeras, T. R. (2013). STAR: ultrafast universal RNA-seq aligner. *Bioinformatics* , *29*(1), 15–21.

Dorszewska, J., Prendecki, M., Oczkowska, A., Dezor, M., & Kozubski, W. (2016). Molecular Basis of Familial and Sporadic Alzheimer's Disease. *Current Alzheimer Research*, *13*(9), 952–963.

Eikelenboom, P., Hoozemans, J. J., Veerhuis, R., van Exel, E., Rozemuller, A. J., & van Gool, W. A. (2012). Whether, when and how chronic inflammation increases the risk of developing late-onset Alzheimer's disease. *Alzheimer's Research & Therapy*, *4*(3). https://doi.org/10.1186/alzrt118

Facts and Figures. (n.d.). Retrieved March 14, 2021, from https://www.alz.org/alzheimers-dementia/facts-figures

Frederic H. Brucato, D. E. B. (2020). Synaptic Pruning in Alzheimer's Disease: Role of the Complement System. *Global Journal of Medical Research*, *20*(6). https://doi.org/10.34257/gjmrfvol20is6pg1

Fusaki, N., Ban, H., Nishiyama, A., Saeki, K., & Hasegawa, M. (2009). Efficient induction of transgene-free human pluripotent stem cells using a vector based on Sendai virus, an RNA virus that does not integrate into the host genome. *Proceedings of the Japan Academy. Series B, Physical and Biological Sciences*, *85*(8), 348–362.

Glass, C. K., Saijo, K., Winner, B., Marchetto, M. C., & Gage, F. H. (2010). Mechanisms underlying inflammation in neurodegeneration. *Cell*, *140*(6), 918–934.

González-Reyes, R. E., Nava-Mesa, M. O., Vargas-Sánchez, K., Ariza-Salamanca, D., & Mora-Muñoz, L. (2017). Involvement of Astrocytes in Alzheimer's Disease from a Neuroinflammatory and Oxidative Stress Perspective. *Frontiers in Molecular Neuroscience*, *10*. https://doi.org/10.3389/fnmol.2017.00427

Gurses, M. S., Ural, M. N., Gulec, M. A., Akyol, O., & Akyol, S. (2016). Pathophysiological Function of ADAMTS Enzymes on Molecular Mechanism of Alzheimer's Disease. *Aging and Disease*, *7*(4), 479.

Hemonnot, A.-L., Hua, J., Ulmann, L., & Hirbec, H. (2019). Microglia in Alzheimer Disease: Well-Known Targets and New Opportunities. *Frontiers in Aging Neuroscience*, *11*. https://doi.org/10.3389/fnagi.2019.00233

Heneka, M. T., Carson, M. J., El Khoury, J., Landreth, G. E., Brosseron, F., Feinstein, D. L., Jacobs, A. H., Wyss-Coray, T., Vitorica, J., Ransohoff, R. M., Herrup, K., Frautschy, S. A., Finsen, B., Brown, G. C., Verkhratsky, A., Yamanaka, K., Koistinaho, J., Latz, E., Halle, A., … Kummer, M. P. (2015). Neuroinflammation in Alzheimer's Disease. *Lancet Neurology*, *14*(4), 388.

Hickman, S. E., Allison, E. K., & El Khoury, J. (2008). Microglial dysfunction and defective beta-amyloid clearance pathways in aging Alzheimer's disease mice. *The Journal of Neuroscience: The Official Journal of the Society for Neuroscience*, *28*(33), 8354–8360.

Hou, L., Liu, Y., Wang, X., Ma, H., He, J., Zhang, Y., Yu, C., Guan, W., & Ma, Y. (2011). The effects of amyloid-β42 oligomer on the proliferation and activation of astrocytes in vitro. *In Vitro Cellular & Developmental Biology. Animal*, *47*(8), 573–580.

Hur, J.-Y., Frost, G. R., Wu, X., Crump, C., Pan, S. J., Wong, E., Barros, M., Li, T., Nie, P., Zhai, Y., Wang, J. C., Julia, T. C. W., Guo, L., McKenzie, A., Ming, C., Zhou, X., Wang, M., Sagi, Y., Renton, A. E., … Li, Y.-M. (2020). The innate immunity protein IFITM3 modulates γ-secretase in Alzheimer's disease. *Nature*, *586*(7831), 735–740.

Kelleher, R. J., 3rd, & Shen, J. (2017). Presenilin-1 mutations and Alzheimer's disease [Review of *Presenilin-1 mutations and Alzheimer's disease*]. *Proceedings of the National Academy of Sciences of the United States of America*, *114*(4), 629–631.

Khakh, B. S., Beaumont, V., Cachope, R., Munoz-Sanjuan, I., Goldman, S. A., & Grantyn, R. (2017). Unravelling and Exploiting Astrocyte Dysfunction in Huntington's Disease. *Trends in Neurosciences*, *40*(7), 422–437.

Kim, Y. S., & Joh, T. H. (2006). Microglia, major player in the brain inflammation: their roles in the pathogenesis of Parkinson's disease. *Experimental & Molecular Medicine*, *38*(4), 333–347.

Kinney, J. W., Bemiller, S. M., Murtishaw, A. S., Leisgang, A. M., Salazar, A. M., & Lamb, B. T. (2018). Inflammation as a central mechanism in Alzheimer's disease. *Alzheimer's & Dementia : Translational Research & Clinical Interventions*, *4*, 575.

Krencik, R., & Zhang, S.-C. (2011). Directed differentiation of functional astroglial subtypes from human pluripotent stem cells. *Nature Protocols*, *6*(11), 1710–1717.

Kuleshov, M. V., Jones, M. R., Rouillard, A. D., Fernandez, N. F., Duan, Q., Wang, Z., Koplev, S., Jenkins, S. L., Jagodnik, K. M., Lachmann, A., McDermott, M. G., Monteiro, C. D., Gundersen, G. W., & Ma'ayan, A. (2016). Enrichr: a comprehensive gene set enrichment analysis web server 2016 update. *Nucleic Acids Research*, *44*(W1), W90–W97.

Le Douce, J., Maugard, M., Veran, J., Matos, M., Jégo, P., Vigneron, P.-A., Faivre, E., Toussay, X., Vandenberghe, M., Balbastre, Y., Piquet, J., Guiot, E., Tran, N. T., Taverna, M., Marinesco,

S., Koyanagi, A., Furuya, S., Gaudin-Guérif, M., Goutal, S., … Bonvento, G. (2020). Impairment of Glycolysis-Derived l-Serine Production in Astrocytes Contributes to Cognitive Deficits in Alzheimer's Disease. *Cell Metabolism*, *31*(3), 503–517.e8.

Liddelow, S. A., Guttenplan, K. A., Clarke, L. E., Bennett, F. C., Bohlen, C. J., Schirmer, L., Bennett, M. L., Münch, A. E., Chung, W.-S., Peterson, T. C., Wilton, D. K., Frouin, A., Napier, B. A., Panicker, N., Kumar, M., Buckwalter, M. S., Rowitch, D. H., Dawson, V. L., Dawson, T. M., … Barres, B. A. (2017). Neurotoxic reactive astrocytes are induced by activated microglia. *Nature*, *541*(7638), 481–487.

Lindberg, C., Selenica, M.-L. B., Westlind-Danielsson, A., & Schultzberg, M. (2005). Beta-amyloid protein structure determines the nature of cytokine release from rat microglia. *Journal of Molecular Neuroscience: MN*, *27*(1), 1–12.

Li, T., Chen, X., Zhang, C., Zhang, Y., & Yao, W. (2019). An update on reactive astrocytes in chronic pain. *Journal of Neuroinflammation*, *16*(1), 140.

Liu, C., Cui, G., Zhu, M., Kang, X., & Guo, H. (2014). Neuroinflammation in Alzheimer's disease: chemokines produced by astrocytes and chemokine receptors. *International Journal of Clinical and Experimental Pathology*, *7*(12), 8342.

Love, M. I., Huber, W., & Anders, S. (2014). Moderated estimation of fold change and dispersion for RNA-seq data with DESeq2. *Genome Biology*, *15*(12), 550.

Ma, J., Ma, C., Li, J., Sun, Y., Ye, F., Liu, K., & Zhang, H. (2020). Extracellular Matrix Proteins Involved in Alzheimer's Disease. *Chemistry* , *26*(53). https://doi.org/10.1002/chem.202000782

Marini, F., & Binder, H. (2019). pcaExplorer: an R/Bioconductor package for interacting with RNA-seq principal components. *BMC Bioinformatics*, *20*(1), 1–8.

Medvedev, S. P., Shevchenko, A. I., & Zakian, S. M. (2010). Induced Pluripotent Stem Cells: Problems and Advantages when Applying them in Regenerative Medicine. *Acta naturae*, *2*(2), 18–28.

Mendez, M. F. (2019). Early-onset Alzheimer Disease and Its Variants. *Continuum* , *25*(1), 34–51.

Neuroinflammation Working Group, Akiyama, H., Barger, S., Barnum, S., Bradt, B., Bauer, J., Cole, G. M., Cooper, N. R., Eikelenboom, P., Emmerling, M., Fiebich, B. L., Finch, C. E., Frautschy, S., Griffin, W. S. T., Hampel, H., Hull, M., Landreth, G., Lue, L., Mrak, R., … Wyss–Coray, T. (2000). Inflammation and Alzheimer's disease. *Neurobiology of Aging*, *21*(3), 383.

Oksanen, M., Petersen, A. J., Naumenko, N., Puttonen, K., Lehtonen, Š., Gubert Olivé, M., Shakirzyanova, A., Leskelä, S., Sarajärvi, T., Viitanen, M., Rinne, J. O., Hiltunen, M., Haapasalo, A., Giniatullin, R., Tavi, P., Zhang, S.-C., Kanninen, K. M., Hämäläinen, R. H., & Koistinaho, J. (2017). PSEN1 Mutant iPSC-Derived Model Reveals Severe Astrocyte Pathology in Alzheimer's Disease. *Stem Cell Reports*, *9*(6), 1885–1897.

Papadopoulos, M. C., Manley, G. T., Krishna, S., & Verkman, A. S. (2004). Aquaporin-4 facilitates reabsorption of excess fluid in vasogenic brain edema. *FASEB Journal: Official Publication of the Federation of American Societies for Experimental Biology*, *18*(11). https://doi.org/10.1096/fj.04-1723fje

Piaceri, I., Nacmias, B., & Sorbi, S. (2013). Genetics of familial and sporadic Alzheimer's disease. *Frontiers in Bioscience* , *5*. https://doi.org/10.2741/e605

Rissman, R. A., De Blas, A. L., & Armstrong, D. M. (2007). GABA(A) receptors in aging and Alzheimer's disease. *Journal of Neurochemistry*, *103*(4). https://doi.org/10.1111/j.1471-4159.2007.04832.x

Santos, R., Vadodaria, K. C., Jaeger, B. N., Mei, A., Lefcochilos-Fogelquist, S., Mendes, A. P. D., Erikson, G., Shokhirev, M., Randolph-Moore, L., Fredlender, C., Dave, S., Oefner, R., Fitzpatrick, C., Pena, M., Barron, J. J., Ku, M., Denli, A. M., Kerman, B. E., Charnay, P., … Gage, F. H. (2017). Differentiation of Inflammation-Responsive Astrocytes from Glial Progenitors Generated from Human Induced Pluripotent Stem Cells. *Stem Cell Reports*, *8*(6), 1757–1769.

Schneider, V. A., Graves-Lindsay, T., Howe, K., Bouk, N., Chen, H.-C., Kitts, P. A., Murphy, T. D., Pruitt, K. D., Thibaud-Nissen, F., Albracht, D., Fulton, R. S., Kremitzki, M., Magrini, V., Markovic, C., McGrath, S., Steinberg, K. M., Auger, K., Chow, W., Collins, J., … Church, D. M. (2016). Evaluation of GRCh38 and de novo haploid genome assemblies demonstrates the enduring quality of the reference assembly. In *Cold Spring Harbor Laboratory* (p. 072116). https://doi.org/10.1101/072116

Siracusa, R., Fusco, R., & Cuzzocrea, S. (2019). Astrocytes: Role and Functions in Brain Pathologies. *Frontiers in Pharmacology*, *10*. https://doi.org/10.3389/fphar.2019.01114

Szklarczyk, D., Gable, A. L., Lyon, D., Junge, A., Wyder, S., Huerta-Cepas, J., Simonovic, M., Doncheva, N. T., Morris, J. H., Bork, P., Jensen, L. J., & Mering, C. von. (2019). STRING v11: protein-protein association networks with increased coverage, supporting functional discovery in genome-wide experimental datasets. *Nucleic Acids Research*, *47*(D1), D607–D613.

The Promise of Induced Pluripotent Stem Cells (iPSCs) | stemcells.nih.gov. (n.d.). Retrieved May 15, 2020, from https://stemcells.nih.gov/info/Regenerative_Medicine/2006Chapter10.htm

van der Lee, S. J., Wolters, F. J., Ikram, M. K., Hofman, A., Ikram, M. A., Amin, N., & van Duijn, C. M. (2018). The effect of APOE and other common genetic variants on the onset of Alzheimer's disease and dementia: a community-based cohort study. *Lancet Neurology*, *17*(5), 434–444.

Verkhratsky, A., & Butt, A. (2013). *Glial Physiology and Pathophysiology*. John Wiley & Sons.

von Mering, C., Jensen, L. J., Snel, B., Hooper, S. D., Krupp, M., Foglierini, M., Jouffre, N., Huynen, M. A., & Bork, P. (2005). STRING: known and predicted protein-protein associations,

integrated and transferred across organisms. *Nucleic Acids Research*, *33*(Database issue). https://doi.org/10.1093/nar/gki005

Wei, Y., Shin, M. R., & Sesti, F. (2018). Oxidation of KCNB1 channels in the human brain and in mouse model of Alzheimer's disease. *Cell Death & Disease*, *9*(8), 1–13.

Weller, J., & Budson, A. (2018). Current understanding of Alzheimer's disease diagnosis and treatment. *F1000Research*, *7*. https://doi.org/10.12688/f1000research.14506.1

Yamanaka, S. (2007). Induction of pluripotent stem cells from mouse fibroblasts by four transcription factors. In *Cell Proliferation* (Vol. 41, pp. 51–56). https://doi.org/10.1111/j.1365-2184.2008.00493.x

Zador, Z., Stiver, S., Wang, V., & Manley, G. T. (2009). Role of aquaporin-4 in cerebral edema and stroke. *Handbook of Experimental Pharmacology*, *190*. https://doi.org/10.1007/978-3-540-79885-9_7

Zalocusky, K. A., Nelson, M. R., & Huang, Y. (2019). An Alzheimer's-disease-protective APOE mutation. *Nature Medicine*, *25*(11), 1648–1649.

Zhu, A., Ibrahim, J. G., & Love, M. I. (2019). Heavy-tailed prior distributions for sequence count data: removing the noise and preserving large differences. *Bioinformatics*, *35*(12), 2084–2092.

2020 Alzheimer's disease facts and figures. Alzheimer's & Dementia. 2020 Mar 10. doi: 10.1002/alz.12068. Epub ahead of print. PMID: 32157811.